



A micromechanical study and uncertainty quantification for effective properties of unidirectional fibre reinforced composites



S. Koley, P.M. Mohite*, C.S. Upadhyay

Department of Aerospace Engineering, Indian Institute of Technology Kanpur, 208016, India

ARTICLE INFO

Keywords:

Composite materials
Microstructure
Randomness
Homogenization theory
Effective properties
Local volume fraction

ABSTRACT

A micromechanical framework is proposed to investigate the effective mechanical properties of elastic two-phase composites with randomly dispersed inhomogeneities in the form of continuous fibres. In this study, an algorithm is developed to generate the microstructure of unidirectional fibre reinforced composite through a three dimensional RVE approach. Using this approach, both regular and random fibre distributions with both undistorted and distorted cross sections are considered and then analysed using mathematical theory of homogenization to estimate the homogenized or effective material properties. Here, RVEs are modeled with random fibre distribution maintaining a fibre volume fraction of 0.6 but increasing the number of fibres gradually and also randomly varying their positions. Finally, the effect of the variation of local volume fraction is studied through master RVE using the moving window technique. The variation in the predicted elastic properties for the given volume fraction for the above-mentioned scenarios is compared with the experimental values. The study shows that results from RVE with more number of random fibres arrangement with geometric cross sectional variations approach the experimental values. However, there is a significant percentage difference in transverse shear moduli, G_{23} and ν_{23} , of about 22% and 35%, respectively with respect to the experimental results for the scenarios with random fibre distribution. Further, about 16% difference in axial modulus E_1 is seen when the effects of local volume fractions are studied.

1. Introduction

Composite materials are extensively used in advanced structural elements in aerospace, automobile and many other industries due to their high strength to weight ratio, high modulus and low density reinforcements [1]. These immense uses of composite materials require accurate prediction of mechanical behaviour and effective elastic properties of fibre reinforced composites. In fibre reinforced composites, fibres are the main load carrying members [2,3]. Therefore, fibre volume fraction and fibre distribution morphology have decisive influence on the strength and stiffness properties of composite materials. To study these effects, micromechanics of composite material has been addressed by many researchers (For example, see [4]). However, there exists one common problem in the mechanics of composite materials, which is to establish a rational microstructure model considering the random distribution of the fibres [5]. In order to analyse the mechanical behaviour an appropriate Representative Volume Element (RVE), representing the microstructure of the composite should be defined first. Therefore, the issue concerning the micromechanical study is the generation of RVE with the desired dimensions. As RVE cannot be too large

or too small as this would assist the possibility to numerically analyse it. However, it should contain a large enough volume that captures the essence of the microstructure of a composite material. Several attempts have been made in literature to develop a procedure to determine the representative volume. Gitman et al. [6] have studied about the determination of RVE size on the basis of statistical analysis and with size effect theory. Kanih et al. [7] demonstrated that different critical RVE sizes exist for different effective properties, such as in the case of thermal conductivity or linear elasticity.

The second issue is the spatial distribution of reinforcements in RVE which highly depends upon the manufacturing process. Some authors (see [8]) have developed computational techniques to simulate composite materials with random distribution of fibres. The probabilistic framework is a well established way for modeling randomness both from theoretical and practical point of view. Many methods have been developed for the generation of RVE model with random distribution of fibres using Poisson point distribution [9], where the points are centres of the fibres. This method faces a problem as it hardly generates the distributions with fibre volume fraction greater than 50%. Some authors have developed stochastic finite element methods like polynomial

* Corresponding author.

E-mail address: mohite@iitk.ac.in (P.M. Mohite).

<https://doi.org/10.1016/j.compstruct.2019.111141>

Received 4 January 2019; Received in revised form 24 May 2019; Accepted 11 June 2019

Available online 14 June 2019

0263-8223/ © 2019 Elsevier Ltd. All rights reserved.

chaos expansion or perturbation methods [10] to retain the main statistics of the response of the random systems. Furthermore, this non-uniformity not only affects effective properties of composite materials but is also a crucial factor in initiation and subsequent development of damage.

To determine the effective properties of a composite one needs to consider the microscale, that is, the scale at which the fibre and matrix are present. In this microscopic scale approach, the constituents are employed in conjunction with homogenization to predict the composite behaviour. Thus, 'homogenization' through numerical methods (e.g. FEM) has been implemented by researchers as a capable method for predicting properties of the material in higher scale using the results of analysis in lower scale [11]. The current trend of work in micromechanics is to estimate the effective elastic properties of the RVE of the material with an equivalent random distribution of fibres [12]. It is a highly attractive process to simulate the real mechanical behaviour of the composite materials through finite element analysis. Effective elastic properties of this heterogeneous structure, i.e. the composite, depend on the size, shape, properties and spatial distribution of the second phase, i.e. the fibre. Among the various uncertainties present, the following uncertainties have been considered for the analysis: (a) volume fraction, (b) randomness in the fibre arrangements and (c) fibre cross-section shape. The influence of manufacturing uncertainties on the composite material property variation is often not characterised properly. Effect of manufacturing induced uncertainty is significantly depend on the corresponding amount of constituent elements and many other factors which are mentioned in [13]. Among others, Yushanov and Bogdanovich [14] highlighted on the uncertainties of fibre curvature and layer arrangement.

In the current study, a micromechanical framework is proposed to investigate effective mechanical properties of elastic composites with regular fibre array (square) and randomly dispersed fibres in a unit cell model [15]. Initially, an algorithm for the automatic generation of 3D RVE model of unidirectional fibre reinforced composite is presented. Uncertainties in composite materials may be built up from a constituent level which is carried out either by simulating the composite material behaviour based on a large number of random variables starting from fibre/matrix properties or by considering the microstructural morphology. This uncertainty in the fibre distribution has been studied, through which we estimate the scatter in the fibre arrangement at macro scale. By using this scatter data, we create more realistic models of the microstructure. To achieve this goal, a comprehensive study is carried out with RVEs having single fibre (replica of the real image), 12 fibres, 20 fibres and 50 fibres. The effect of this random distribution has been validated with the experimental results reported in [16]. The performances of different fibre arrays in various aspects are compared including the prediction of effective properties, stress concentration factors, matrix rich and fibre cluster regions, which in most cases contribute to failure initiation. Further, RVEs with fibres randomly distributed in a periodic unit cell but with different fibre cross sections are considered and studied how these different fibre cross sections affect the mechanical properties. Finally, it has been studied how the variation in the local volume fraction affects the effective elastic properties at different positions inside the RVE due to the random distribution of the fibres. Here, two RVE models are considered. In the first RVE model we fixed the window size and then this window is moved throughout the RVE to estimate the effective properties. In the second RVE model, different sizes of the window are chosen and they are moved throughout the RVE to estimate the effective properties.

The main motivation for this work is that single fibre unit cell data is not good enough as the computed single fibre unit cell properties are at great variance with the experimental results mainly the shear properties. This is because the shielding effect of neighbouring fibres is not seen in this RVE. This is one of the reasons for modelling of multi-fibre RVE. However, the issue over multi-fibre RVE is the statistical homogeneity as the obtained properties should be independent of the RVE

size. Based on the literature by Gitman et al. [6] and Kanit et al. [7], the size of the RVE has been decided which will be sufficient for doing the micromechanical analysis, that is a statistically equivalent RVE with more fibres is constructed. Unlike most studies reported in literature, here three dimensional RVEs are analysed. On the basis of literature, RVEs are modeled with a maximum of 50 fibres. The main focus here is to carry a systematic study of RVE's of different sizes obtained by varying the number of fibres and cross section shape. Statistically converged (i.e. with almost zero variance) RVE analysis based properties will be compared to experimental results. Thus we build in randomness in spatial distribution of fibres, variation in the fibre cross section and also the size of the RVE (through change in number of fibres in the RVE). This is possibly the most comprehensive study of its kind. The result clearly indicate what predictions can be obtained by the homogenization method, and also identify the variance between the computational and experimental results.

Remark: The experiment results, with which the obtained results are compared, must have been obtained with a certain reliability and are the outcome of a comprehensive study [17]. The experimental data depends upon (a) Amount of available data, (b) quality of the available data, (c) type of experiments conducted and (d) possible limitations.

Remark: Micromechanics gives all the effective material properties for the composite with only the assumption of periodicity. A plane strain analysis is a simplification, that will give the transverse properties with good accuracy, but not the ones in the fibre direction, i.e. E_1 , G_{13} , ν_{13} , etc. This is one of the reason why we have done three dimensional (3D) RVE analysis, which cannot be achieved by doing a single plane strain model. The 3D-analysis allows us to look at effect of (periodic) micro-damage, fibre waviness and voids easily. Thus, this gives us a more general micro-mechanical tool. The (3D)-analysis also takes care of Poisson's ratio well.

However, for the data used here, from Soden et al. [16], for comparison and validation such information is not available. The data set provided in [16] has become the accepted experimental benchmark.

2. Characterization of uncertainties in composites

The complex manufacturing processes of the composite render randomness in the material parameters. The variability in fibre distribution, volume fraction measurements result in variability of stiffness and strength, which in turn, results in the variability of response of composite materials. In the composite structures, these uncertainties can be addressed by means of material, geometric and structural considerations [9]. The material and geometric uncertainties mainly arise due to lack of control over the manufacturing and fabrication techniques.

The manufacturing of composites is strongly influenced by the volume fractions of its constituents, i.e. fibre (V_f) and matrix (V_m) and the distribution of fibres in the matrix material. The randomness of the fibre distribution in the matrix also depends on curing technique. This spatial arrangements of the reinforcement plays a vital role in the transverse constitutive behaviour of polymer matrix composites. In Fig. 1, an example of real composite microstructure SEM image, which vividly demonstrates the random patterns in the distribution of reinforcements, is shown. From these real microstructures one can model the non uniform arrangement of fibres. This modeling includes the characterization of the microstructure, statistical analysis of the microstructure, construction of the RVE model with random arrangement of fibres and micromechanical modeling of the resulting RVE. Initially, we estimate the scatter in the fibre distribution for these digital images and analyses is carried out on the original image. The grey level image and binary image are obtained from the real microstructure. Using these data, we are able to extract the information about the location of centres of the fibres, the distribution of fibre radius and the distance between neighbouring fibres. Then the obtained statistical parameters are utilized to construct a statistically equivalent RVE based on certain

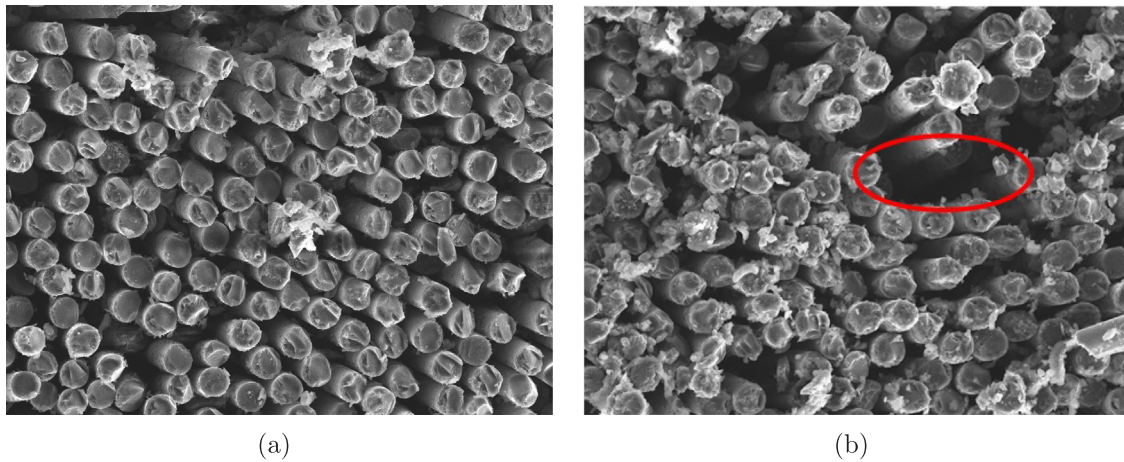


Fig. 1. Distribution of continuous fibres in epoxy matrix in a transverse cross-section of a unidirectionally reinforced ply (digitalisation of a micrograph). (a) SEM micrograph showing random arrangement of fibres, (b) SEM micrograph showing matrix rich region.

numerical algorithms [18].

Fig. 2 is a micrograph image of composite microstructure of size 706×678 pixels, which is first converted into a binary image. From the binary image the volume fraction is calculated by counting the pixels covered by fibre (white circles) compared to the overall size of the image. The fibre volume fraction (V_f) obtained was about 0.65. The representative volume element (RVE) of the composite is calculated using moving window technique. Different window sizes are considered and the volume fraction is calculated for each window. Fig. 3 shows moving window technique which is used to estimate the volume fraction of a given window. The absolute error $|e|$ in the mean value for different window sizes are depicted in Table 1. It is noticed that, with increase in the window size the absolute error value is reduced.

From this random binary image of the composite microstructure, the total count and average radius of the fibres are calculated. The total count of the fibre was 204. From Fig. 3(a), four random fibres are chosen in every window and an ideal distribution of fibres is built along the breadth. Using the mentioned data, the ideal number of fibres along the breadth is estimated to be 14 (see Fig. 3(b) with red dots). The fibre centre (x, y) coordinates of these 14 fibres are considered as the ideal coordinates which are further used to estimate the scatter (S). Fig. 3(b) also shows centres of ideal fibre distribution. Once both actual and ideal coordinates are obtained, the deviations of centres of the fibres in

original micrograph are then calculated. Table 2 shows the scatter data which is calculated by using the expression.

$$\text{Scatter}(S) = \sqrt{(x_{\text{actual}} - x_{\text{ideal}})^2 + (y_{\text{actual}} - y_{\text{ideal}})^2} \quad (1)$$

Thus, the scatter is estimated to give an idea of how the fibres are distributed across the cross-section. Finally, with reference to this RVE, the random distribution of fibres are modeled keeping the required volume fraction constant.

3. Generation of RVE

In the estimation of effective properties of composite materials using finite element techniques, the generation of an RVE plays a vital role. Understanding the considerable deviations of microstructures of real composites from the ideal ones resulted in an introduction of a microstructure into numerical schemes. The two principle ways of modeling the micro-structure are: (1) Direct use of scanned image of microstructure and (2) Generation of an artificial microstructure. To generate a statistically equivalent RVE, the random sequential adsorption technique has been widely used, which creates randomly distributed points inside a region, with a constraint that no pair of points may be closer than a certain minimum distance. However, this technique does not permit the fibre volume fraction to be greater than 54.7%

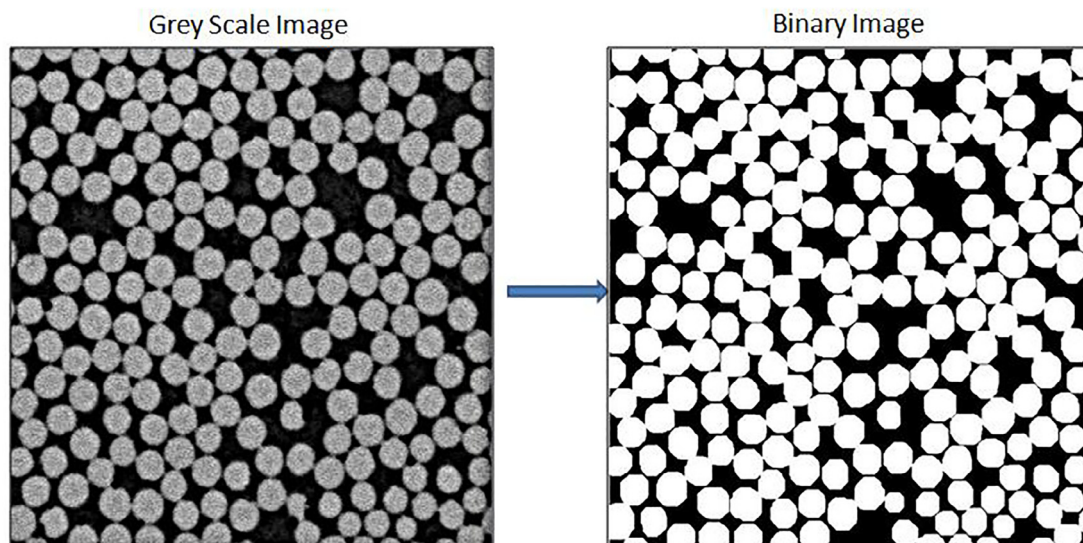


Fig. 2. Conversion of a grey scale image to binary image.

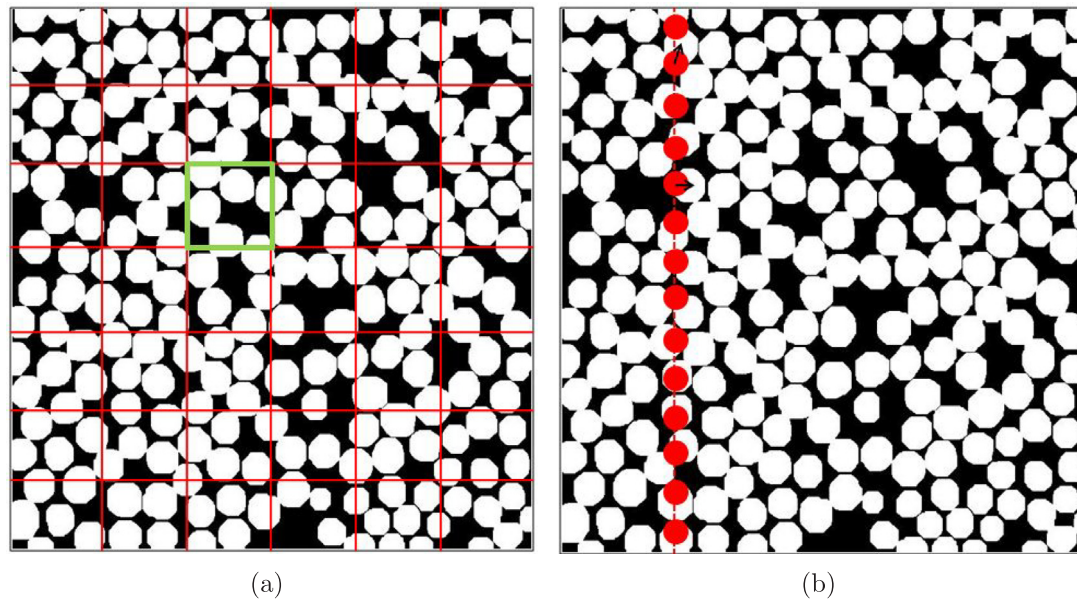


Fig. 3. Fibre distribution to estimate the scatter. (a) Moving window technique used to calculate RVE, (b) Deviations of fibres from their ideal distribution.

Table 1
Absolute error in mean value of (V_f) for different window sizes.

Window size	$ e $ in mean value of (V_f)
47 × 47	0.10
94 × 94	0.06
141 × 141	0.05
188 × 188	0.04
235 × 235	0.02
282 × 282	0.03

because of “jamming limit”. Melro et al. [19] developed a three step procedure for the generation of random fibre distribution and their algorithm has the capability of achieving a fibre volume fraction of 65%. Yang et al. [20] proposed random distributions for various fibre volume fractions through adjusting the inter fibre distance parameters which results in fibre aggregation in the centre area and matrix rich regions at the corners. In order to generate a statistically equivalent RVE for a composite microstructure of high fibre volume fractions, initially we consider the micrograph of a single fibre which is then transformed into a computer recognizable format by using binary image processing technique. Fig. 4(a) shows the micrograph with single fibre. From this binary image, we estimate diameter of the fibre and fibre volume fraction, which are approximately $6.72 \pm 0.25 \mu\text{m}$ and about 60%,

Table 2
Scatter data of fibres from their ideal positions.

Actual Coordinates		Ideal Coordinates		Displacement		Scatter
x_{actual}	y_{actual}	x_{ideal}	y_{ideal}	$(x_{actual} - x_{ideal})$	$(y_{actual} - y_{ideal})$	(S)
148.63	616.71	148.40	587.93	0.23	28.78	28.78
146.27	641.33	148.40	611.86	-2.12	29.46	29.54
156.64	566.24	148.40	564.80	8.24	1.44	8.36
148.58	522.57	148.40	517.73	0.18	4.84	4.84
149.06	477.91	148.40	470.66	0.66	7.25	7.28
134.54	432.72	148.40	423.60	-13.89	9.12	16.62
163.68	393.75	148.40	376.53	15.28	17.21	23.02
168.75	336.39	148.40	329.46	20.35	6.93	21.49
143.20	291.87	148.10	282.40	-5.19	9.47	10.80
163.68	229.48	148.10	235.33	15.28	-5.84	16.36

respectively.

Using this data three dimensional RVE is modeled with single fibre maintaining a fibre volume fraction of 0.6 as shown in Fig. 4(b). However, to consider it as an RVE, it should inherit certain characteristics. According to Hill [21], representative volume should have two main properties: Its structure is “entirely typical” for the composite and it should contain a “sufficient number” of microstructure elements so that boundary conditions at the surface of the composite do not affect its effective properties. The RVE is a volume of a material whose effective behaviour is representative of (and indistinguishable from) that of the material as a whole. Thus, the RVE is modeled in such a way that it contains a large sufficient volume in order to capture the essence of the microstructure from a statistical standpoint. The RVE must ensure a given accuracy of the overall estimated properties obtained by spatial averaging of the stress, strain or the energy fields. In particular, it is now clear that the RVE size increases with the non-linearity of the considered behaviour. Several studies have been attempted to define an RVE for different purposes. See [22,23] for more details.

Considering the above characteristics for generating an RVE, the RVEs with random arrangement of fibres are generated. Here, the micrograph of random fibre distribution is transformed into a computer-recognizable format by using image processing technique. From these micrographs of both single fibre as in Fig. 4(a) and random fibre distribution as in Fig. 2, the centres of the fibres and the corresponding required dimensions are obtained. Further, the scatter in the distribution is also estimated. With reference to the scatter from these

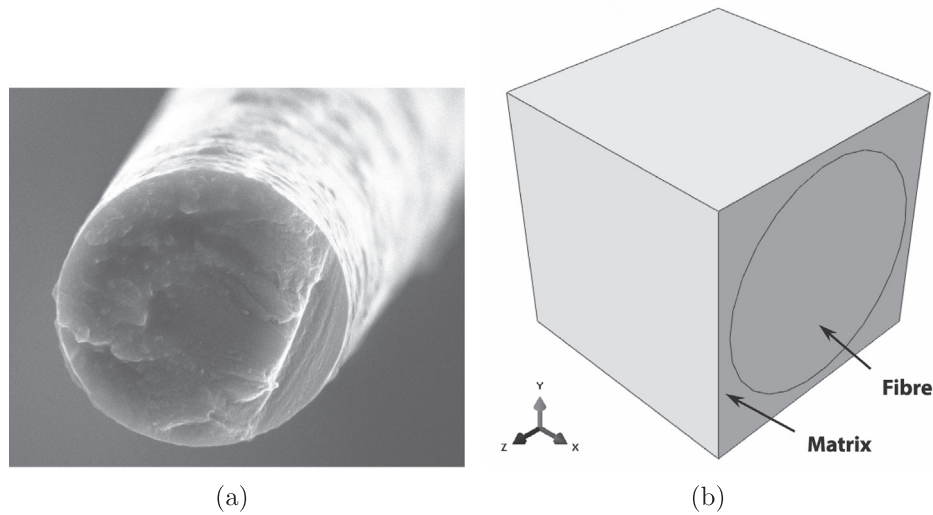


Fig. 4. SEM image of single fibre. (a) Fibre cross section, (b) RVE with single fibre.

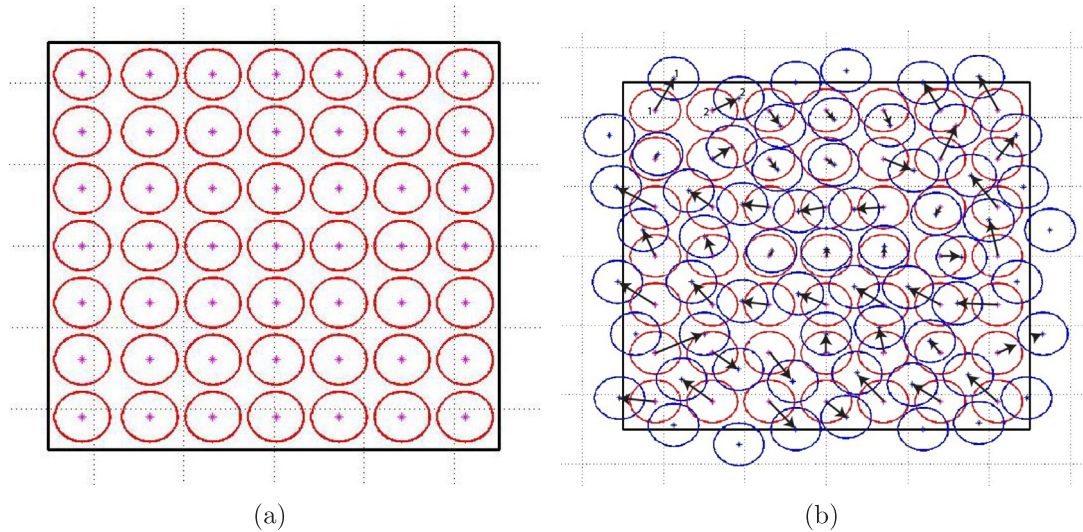


Fig. 5. RVE with regular and random fibre distribution. (a) Regular fibre arrangements in a square domain, (b) Scatter of fibre distribution from regular to random arrangement.

micrographs, the RVEs in Fig. 2 are modeled with ideal/regular arrangements of fibres as shown in Fig. 5 by maintaining the fibre volume fraction of 0.6. Fig. 5(a) shows the regular arrangement of fibres and Fig. 5(b) shows the random arrangement of fibres which makes an offset from the ideal position. With regular arrangement of fibres an RVE with 49 fibres was generated.

From the SEM images, the diameters of the fibre cross sections were obtained. With this information, the RVE is modeled with regular array maintaining the fibre volume fraction of 0.6. Here, all the fibres in an RVE are considered to be straight and parallel to each other. The algorithm for generation of an RVE is briefly presented here:

1. Step 1: The first fibre is generated at the centre of the domain and then taken as the 'current fibre'.
2. Step 2: If the distance between the new fibre and the previously generated fibres is greater than the prescribed minimum distance then, the new fibre will be generated.
3. Step 3: The periodicity of fibre is maintained to ensure material continuity across the boundaries when multiple RVEs are arranged for the generation of macrostructure, since RVE is locally periodic.
4. Step 4: The volume fraction is updated each time a newly generated random fibre is placed inside the cube satisfying the above criteria.

5. Step 5: Once the rearrangement of fibres is done, fibres positioned along the edges of the RVE are pushed inwards, always maintaining the minimum distance between the fibres and not overlapping with the neighbouring fibres.

The flowchart for the three-dimensional (3D) RVE generation with regular distribution of fibre with the updation of fibre is shown in Fig. 6.

RVEs with regular fibre distribution were generated. Now, to model the RVE with random fibre distribution, these regular fibres are displaced randomly both in x and y – directions. This arrangement is restricted to a prescribed minimum distance so that the fibres do not intersect each other and also maintain the periodicity at the edges of the domain as shown in Fig. 5(b). Once the RVE is generated with random fibre distribution, the scatter is measured with respect to the regular arrangement. The RVE possesses very similar microstructural features as in the original micrograph such as resin rich region, fibre aggregation zones while maintaining the geometric periodicity of the RVE.

3.1. Geometric periodicity

One of the major assumptions of RVE is that the model is

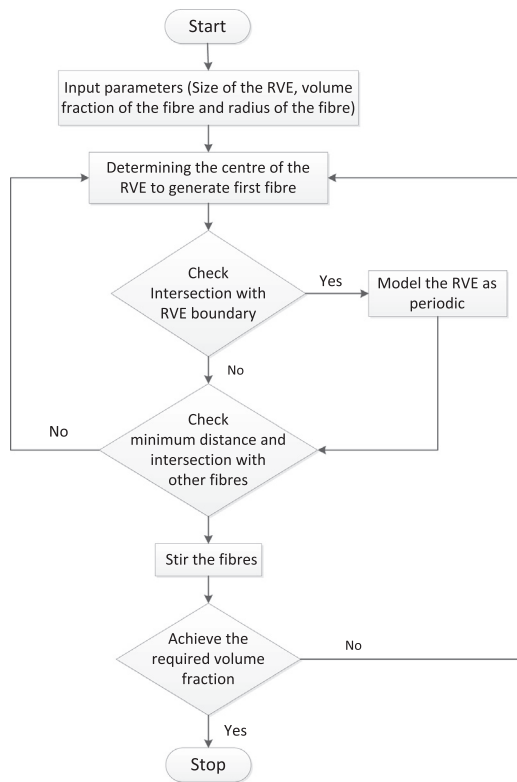


Fig. 6. Algorithm to generate regular fibre arrangement in an RVE.

geometrically periodic in nature. The geometric periodicity can also be explained as the periodicity of materials. For each reinforcement element that intersects the boundaries of the cell, a set of matching geometries is created in order to guarantee cell-to-cell continuity. Therefore, by replicating RVE in three perpendicular directions one should be able to form the actual structure. In the following, the implementation of periodicity across faces, edges and corners are explained in brief.

3.2. Periodicity across faces

Periodicity across faces is implemented to maintain the continuity of fibres across the faces of an RVE when a fibre crosses a face. The following procedure is incorporated to build the periodicity of an RVE across a face. It must be noted that the fibres that are crossing across the face of a parent cell are shared by another adjacent virtual cell. Fig. 7(a) shows that fibres are at the interior of the RVE which are periodic with the adjacent front and rear unit cells. Thus, periodicity across the faces, i.e. front and rear (y - z) plane of the RVE is considered (see Fig. 7(b)).

The common intersection between cylindrical fibre and faces of an RVE need to be circular in shape as the fibres are unidirectionally arranged. There are no inclusions across the edges and this should be considered as a mere coincidence.

3.3. Periodicity across edges

The fibres can cross the boundary of an RVE through the edges. Here, edges represent the faces of RVE which are parallel to the fibres. The continuity of a fibre across the edge of an RVE is ensured, if the fibre passes across the edge of an RVE. A random arrangement of fibres in cell may lead the fibres to cross the edge of a cell. Considering Fig. 8(a), to I samples are taken as unit cells, with fibres crossing the edge between the sample B and E and sample D and E. Now to make the sample E to be periodic, the portion of fibre from sample D should sit along the edge shared by samples E and F. Similarly, for the fibre

crossing the edge between the sample B and E, the portion of fibre present in sample B should sit along the edge shared by samples E and H. This makes sample E a periodic unit cell, as shown in Fig. 8(b).

By placing cell E on all the four sides of the parent unit cell for periodicity, i.e. the cross section in a bigger view, one obtains the bigger cell of Fig. 8(c).

3.4. Periodicity across corners

When fibres are sequentially arranged in a unit cell, there is a possibility that fibres can cross the boundary of the cube through its corner (formed due to intersection of the RVE faces parallel to the fibres). A fibre crossing the boundary of a parent cell through its corner is shared by four adjacent virtual cells. There are two possibilities: In the first, the centre of a fibre exactly matches with the corner of the cell and in the second, it is offset by some distance. Both these cases are discussed here. Fig. 9(a) shows when the fibre centre exactly matches the corner of the cell samples A, B, E and D. Then to make the unit cell E to be periodic, the portion of fibre shared by the sample D will sit at the north-east corner of the cell E. Similarly, the portion of fibre shared by the sample A will sit at the south-east corner of the cell E and the portion of fibre shared by the sample B will sit at the south-west corner of the cell E. This completes the geometrically periodic construction of the unit cell E, as shown in Fig. 9(b).

The second case, the fibre centre is offset by some distance from the corner of the unit cell, is shown in Fig. 9(c). Here, the same concept is used and the periodic unit cell is shown in Fig. 9(d). Using this method, a sample RVE is constructed in Fig. 10(a), with the assembled bigger microstructure shown in Fig. 10(b).

4. Micromechanical analysis

A primary task in mechanics of materials is the prediction of material behaviour, i.e. to estimate the effective (or overall) properties of the composition, commonly referred to as *homogenization*. The simplest method leading to the homogenized moduli of a heterogeneous material is the rule of mixtures. The overall properties are then calculated as an average over the respective properties of the constituents. The asymptotic homogenization theory [24,25] applies an asymptotic expansion of displacement and stress fields on the length parameter, which is the ratio of the characteristic size of the heterogeneities to the measure of the macrostructure [26]. The asymptotic homogenization approach estimates overall effective properties as well as local stress and strain values. Here, we consider a linearly elastic isotropic matrix reinforced by transversely isotropic, unidirectionally aligned, randomly located continuous fibres. Moreover, we assume that the composite specimen has perfect interfacial bonding between matrix and fibre.

The overall properties of composite are, therefore *transversely isotropic*. Here, carbon fibre (T300 carbon fibre) in epoxy matrix is considered for the estimation of effective properties. The advantage of the micromechanical approach is that it allows not only estimation of effective properties of composites but also stress/strain concentration factors which can be used in damage initiation and propagation study. Micromechanical analysis calculates the local stress and strain distribution in the material followed by a volumetric averaging procedure to obtain effective properties. Effective linear elastic modulus tensor, $\bar{\mathbf{C}}$, for a heterogeneous material is defined as the tensor relating the average strain, $\bar{\boldsymbol{\varepsilon}}$, to the average stress, $\bar{\boldsymbol{\sigma}}$, as

$$\bar{\sigma}_{ij} = \bar{C}_{ijkl} \bar{\varepsilon}_{kl} \quad (2)$$

The prediction is obtained by solving a boundary value problem on the RVE. The boundary conditions are either traction or displacement type on the boundary of RVE, ∂V_{RVE} , i.e.

$$\bar{t}_i = \sigma_{ij}^{(0)} n_j \text{ for traction} \quad (3)$$

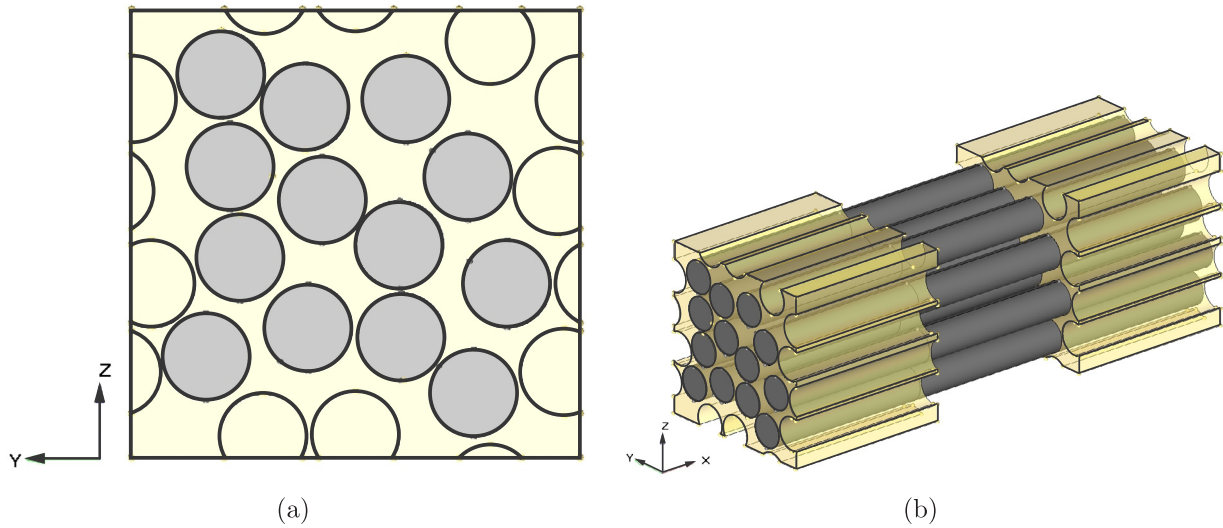


Fig. 7. Distribution of continuous fibres in epoxy matrix in a transverse cross-section of a unidirectionally reinforced ply. (a) Front view of the RVE showing fibres interior of the RVE, (b) Isometric view showing fibres passing throughout the RVE which shows periodicity across faces.

$$u_i = \varepsilon_{ij}^{(0)} n_j \text{ for displacement} \quad (4)$$

where, $\sigma_{ij}^{(0)}$ and $\varepsilon_{ij}^{(0)}$ are the applied macro stresses and applied macro strains, respectively. Random arrangement of fibres in the matrix results in \bar{C} to be isotropic in the transverse (cross sectional) plane. The macro-stress and macro-strain are derived by averaging stress and strain tensors over the volume of the RVE as

$$\bar{\varepsilon}_{ij} = \frac{1}{V_{RVE}} \int_{V_{RVE}} \varepsilon_{ij} dV \quad (5)$$

$$\bar{\sigma}_{ij} = \frac{1}{V_{RVE}} \int_{V_{RVE}} \sigma_{ij} dV \quad (6)$$

where, σ_{ij} and ε_{ij} are the local stresses and local strains, respectively and V_{RVE} is the volume of the periodic representative volume element.

In this study, we use continuum approach to determine the effective properties of the composites. In micro mechanics based method the local level and global level analyses are decoupled. The local level analysis considers the microstructural details in its modeling and this analysis gives the effective elastic properties. Further, this local level analysis can be used to calculate the effective or average RVE strain from the local strain within the RVE. This approach has been used to estimate the effective properties in a method termed as ‘mathematical theory of homogenization’ by Suquet [27], as described briefly in the next section.

4.1. Mathematical theory of homogenization

This theory establishes mathematical relations between micro-fields

and macro-fields [28], using a multi-scale perturbation method. The effective properties naturally emerge as a consequence of these relations. The local displacement field in the cell is given as

$$u_i^\Delta(\mathbf{x}\mathbf{y}) \approx u_i^{(0)}(\mathbf{x}) + \Delta u_i^{(1)}(\mathbf{y}) \quad (7)$$

where, \mathbf{x} is the actual coordinate, \mathbf{y} is the scaled unit cell coordinate, $u_i^{(0)}(\mathbf{x})$ is the macro response, $u_i^{(1)}(\mathbf{y})$ is the periodic micro correction and Δ is the ratio of microstructure size to the total size of analysis region ($\Delta = \frac{x}{y}$). $u_i^{(1)}(\mathbf{y})$ can be obtained from each of the six fundamental macro-strains ε_{ij}^x , where

$$\varepsilon_{ij}^x = \frac{1}{2} \left(\frac{\partial u_i^{(0)}}{\partial x_j} + \frac{\partial u_j^{(0)}}{\partial x_i} \right) \quad (8)$$

by solving the periodic cell problem,

$$-\frac{\partial}{\partial y_j} (C_{ijkl}^\Delta \varepsilon_{kl}^y(\chi^{rs})) = \frac{\partial}{\partial y_j} (C_{ijrs}(\mathbf{y})) \quad (9)$$

where, χ^{rs} is \mathbf{y} periodic and

$$\varepsilon_{ij}^y(\chi^{rs}) = \frac{1}{2} \left(\frac{\partial(\chi_i^{rs})}{\partial y_j} + \frac{\partial(\chi_j^{rs})}{\partial y_i} \right) \quad (10)$$

The above equation is obtained by assuming the general solution of the micro problem, $u_i^{(1)}(\mathbf{y})$, of the following form

$$u_i^{(1)}(\mathbf{x};\mathbf{y}) = \chi^{rs} \varepsilon_{rs}^x(\mathbf{v}_0(\mathbf{x})) \quad (11)$$

The above expression implies that the micro solution is expressed as a combination of solutions corresponding to individual macrostrains ε_{rs}^x ,

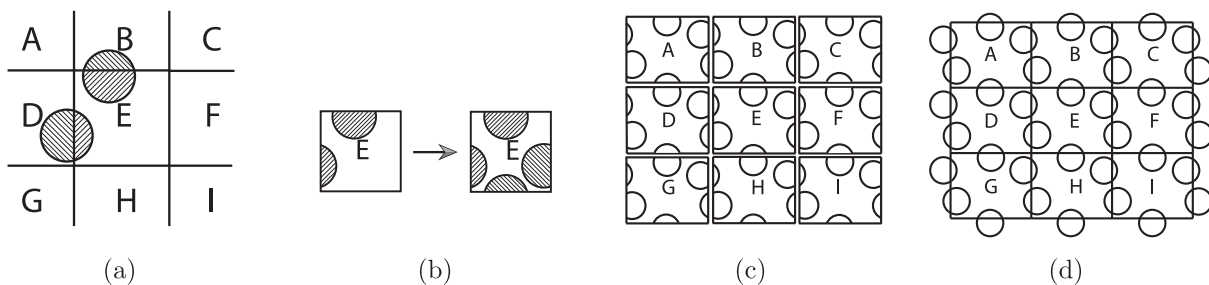


Fig. 8. Modeling of edge periodicity in unit cell. (a) Fibre crossing the edges of unit cell, (b) Unit cell with geometric periodicity, (c) Multiple fibres crossing the edges of the RVE, (d) Unit cell with edge periodicity.

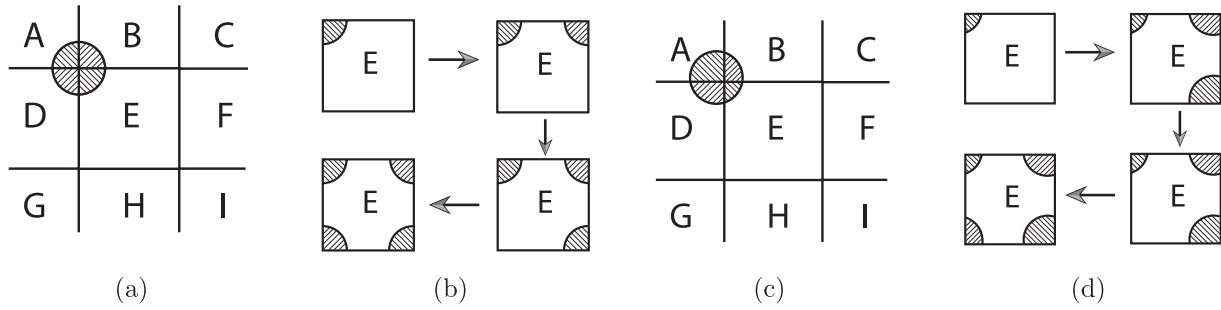


Fig. 9. Modeling of corner periodicity in unit cell. (a) Fibre centre is at the corner of the unit cell, (b) Unit cell showing periodicity at the corner, (c) Fibre centre is offset to a distance from the corner of the unit cell, (d) Unit cell showing periodicity at the corner when fibre is offset.

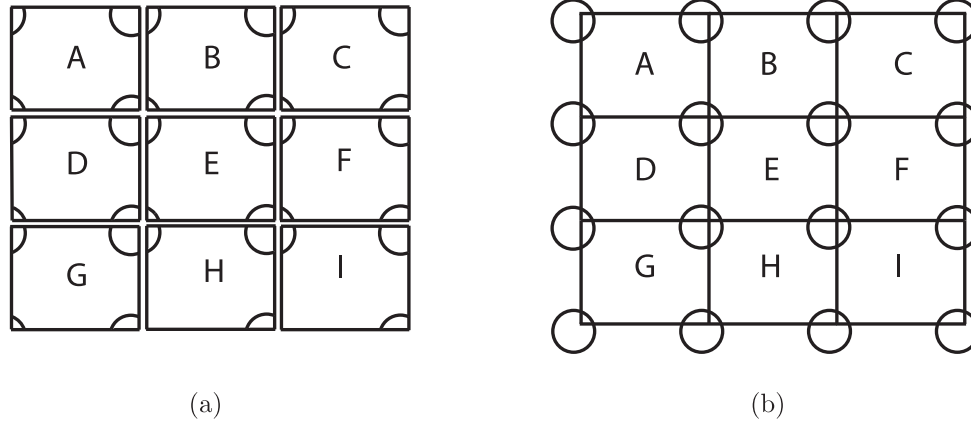


Fig. 10. Periodicity at the corner of the unit cells on bigger cross section. (a) RVEs showing the fibre cross sections at every corner with periodicity, (b) Multiple fibres crossing the corner of the unit cell with periodicity at the corner.

Table 3
Mechanical properties of AS4 carbon fibre material by Soden et al. [16].

E_1 (GPa)	E_2 (GPa)	G_{12} (GPa)	G_{23} (GPa)	ν_{12}
225	15	15	7	0.2

Table 4
Mechanical properties of 3501-6 epoxy matrix material by Soden et al. [16].

E (GPa)	G (GPa)	ν
4.2	1.567	0.35

where $\mathbf{v}_0(\mathbf{x})$ is the periodic solution which is a function of slow variable \mathbf{x} only. From the periodic solution, the total strain $\epsilon_{ij}(\mathbf{u}) \approx \epsilon_{ij}^x(u_i^{(0)}) + \epsilon_{ij}^y(u_i^{(1)}) \approx (1 + M_{ijkl})\epsilon_{kl}^x(u_i^{(0)})$, where M_{ijkl} are the point-wise influence functions and depend on ν_f at the level of the cell [29]. More details can be seen in [30,31]. M_{ijkl} can be expressed as

$$M_{ijkl} = \frac{1}{2} \left(\delta_{ik} \delta_{jl} + \delta_{il} \delta_{jk} \right) - \epsilon_{ij}^y \quad (12)$$

where, δ_{ij} is the Kronecker delta. The effective stiffness tensor which relates average stress and average strain can be calculated from M_{ijkl} by applying Hooke's law at microscopic level and integrating it over the volume of RVE and then dividing by the volume of RVE. Thus,

$$\bar{\sigma}_{ij} = \frac{1}{V_{RVE}} \int_{V_{RVE}} C_{ijpm} M_{pmkl} dV_{RVE} \bar{\epsilon}_{kl} \quad (13)$$

from which the effective stiffness tensor can be written as

$$\bar{C}_{ijkl} = \frac{1}{V_{RVE}} \int_{V_{RVE}} C_{ijpm} M_{pmkl} dV_{RVE} \quad (14)$$

4.2. Computer implementation

In the present work, an in-house finite element code was developed in order to determine the effective homogenized properties of composite materials using mathematical theory of homogenization. Perturbation technique has also been implemented to generate RVEs using MATLAB. In the RVE generation algorithm, fibres are modeled as a line segment in a cube or cuboid. By using the information generated in MATLAB, the commercial software HYPERMESH® is used to generate a solid RVE model satisfying the periodicity condition. The RVEs are discretized with linear tetrahedron elements. The tetrahedron elements are formed from a two dimensional (2D) triangular elements on the boundary. The commercial meshing software HYPERMESH® is used to discretize the RVEs. Initially, a solid RVE is meshed on one side of the surface of cube using two dimensional (2D) triangular elements and the same elements get duplicated and translated to the opposite face to maintain the periodicity. Similar procedure is followed for the fibre elements also. A displacement based finite element formulation has been implemented. A preconditioned conjugate gradient based solver is developed to solve the resulting system of equations. The three dimensional (3D) model is utilized to predict all the elastic constants of the resulting carbon fibre reinforced epoxy composite.

5. Results and discussion

In this section, the effect of randomness in fibre arrangement, number of fibres in RVE and uncertainty in fibre cross section on the effective properties of RVE are discussed. Further, the effect of variation

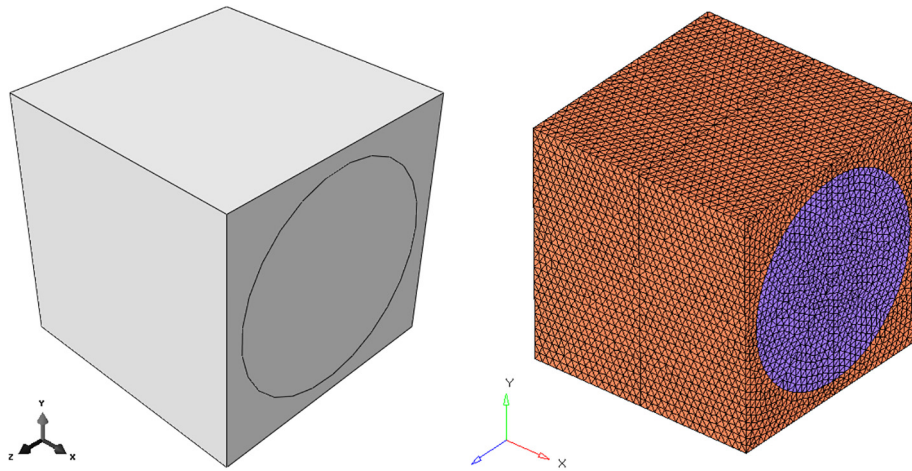


Fig. 11. RVE with single fibre.

Table 5
Effective properties of RVE model with single fibre of T300 and 3501-6 Epoxy.

V_f	E_1 (GPa)	E_2 (GPa)	E_3 (GPa)	G_{12} (GPa)	G_{13} (GPa)	G_{23} (GPa)	ν_{12}	ν_{13}	ν_{23}
0.60	139.58	9.55	9.55	4.70	4.70	3.06	0.25	0.25	0.26

Table 6
Effective properties of T-300/3501-6 epoxy composite (experimental results) [16].

V_f	E_1 (GPa)	E_2 (GPa)	G_{12} (GPa)	G_{23} (GPa)	ν_{12}	ν_{23}
0.60	138	11.00	5.50	3.93	0.28	0.40

of local volume fraction on effective properties is also studied. To study these effects, different scenarios are considered which are discussed in the following. The material modeled here is a typical carbon fibre reinforced epoxy, whose constituent elastic properties are given in Tables 3 and 4. The fibre is transversely isotropic and matrix is isotropic in nature.

The focus of these analyses is to study the longitudinal, transverse and shear behaviour of the material. It is to be noted that the fibre - matrix interface is not modeled in the present study. Here, analyses have been done by considering three different scenarios. Initially, the fibres are modelled as parallel cylinders of constant diameters. Secondly, keeping the fibre diameter approximately same the fibre cross-sections are randomly distorted. Finally, elliptical cross-section of

Table 7
Effective properties of RVEs with twelve fibres (see Fig. 12).

Model	E_1 (GPa)	E_2 (GPa)	E_3 (GPa)	G_{12} (GPa)	G_{13} (GPa)	G_{23} (GPa)	ν_{12}	ν_{13}	ν_{23}
RVE 1	138.19	8.77	8.88	4.51	4.81	3.57	0.25	0.25	0.26
RVE 2	138.70	8.96	8.88	4.91	4.67	3.52	0.25	0.25	0.31
RVE 3	138.54	9.06	9.01	5.06	4.86	3.50	0.25	0.25	0.30
(μ)	138.48	8.93	8.93	4.83	4.78	3.53	0.25	0.25	0.29
(σ)	0.26	0.15	0.07	0.28	0.10	0.03	0.00	0.00	0.03
(ζ)	0.19	1.68	0.78	5.80	2.09	0.85	0.00	0.00	10.34

the fibre is considered keeping the position of the fibre constant. Further, in all these cases the fibres are randomly distributed.

5.1. Case I: Prediction of the elastic constants of RVE with single fibre (circular cross section)

RVE of dimension, approximately $(1.442d \times 1.442d \times 1.442d)$ is modeled with single fibre and the fibre volume fraction of 0.6. Here, d is the diameter of the fibre. The RVE is shown in Fig. 11. This RVE is discretized with 1, 32, 816 elements and 25, 323 nodes. The finite element solution of the problem will require obtaining solutions of the linear system of the form $Ku = b$. It is to be noted that the solutions have to be obtained for all six load cases. Effective properties of the RVE with single fibre are estimated and the results are tabulated in Table 5.

As part of World Wide Failure Exercise, a set of composite laminae and constituent mechanical properties are made available by Hinton et al. [17]. Mechanical properties for the composite laminae were

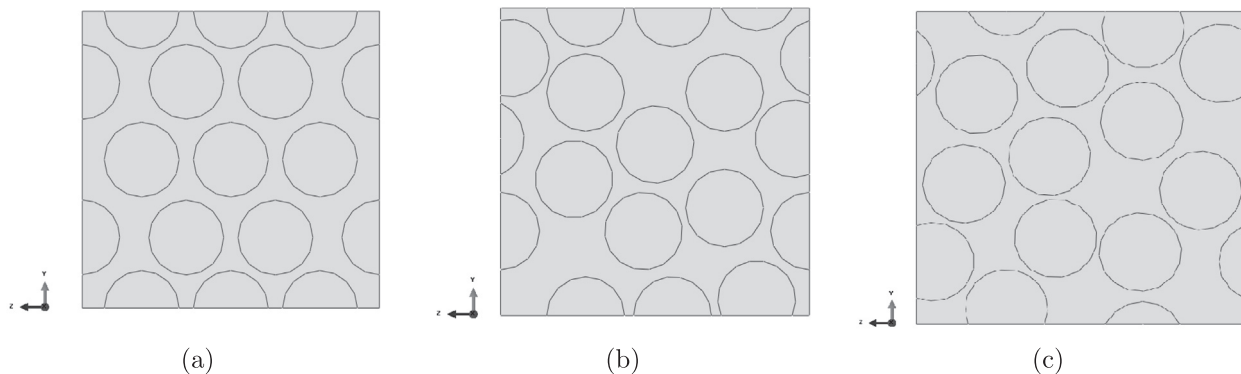


Fig. 12. Representative volume elements with 12 fibres. (a) RVE 1, (b) RVE 2 and (c) RVE 3.

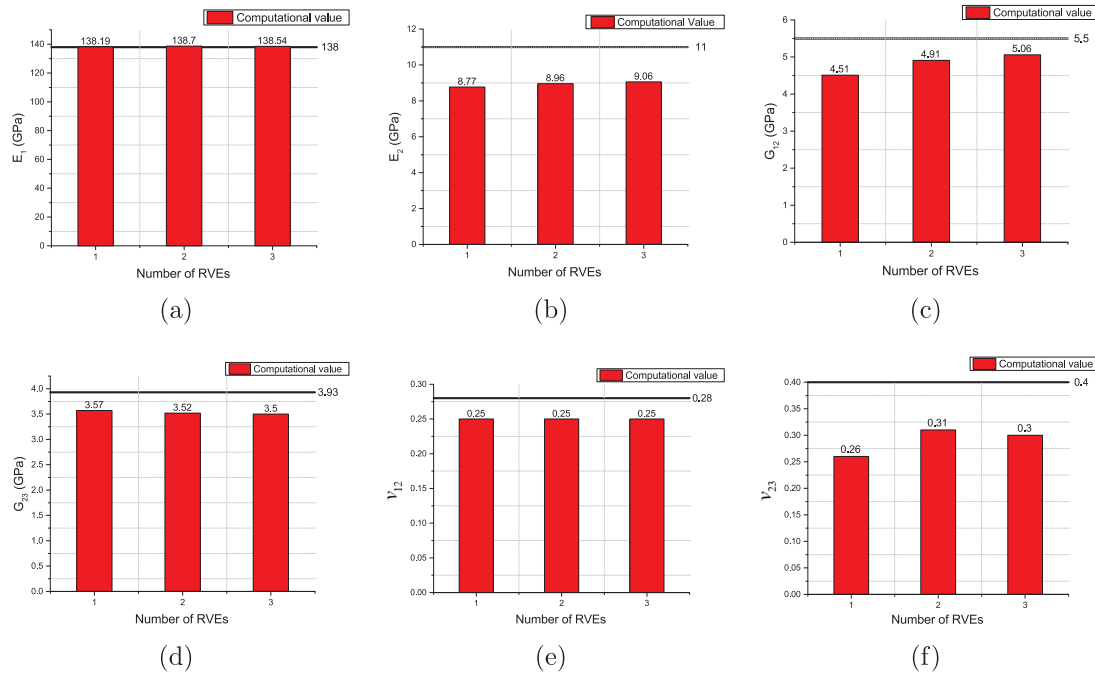


Fig. 13. Elastic constants with respect to experimental value for RVEs with 12 fibres. (a) Longitudinal modulus E_1 , (b) Transverse modulus E_2 , (c) Inplane shear modulus G_{12} , (d) Transverse shear modulus G_{23} , (e) Inplane Poisson's ratio ν_{12} , (f) Transverse Poisson's ratio ν_{23} .

Table 8

Percentage change (φ_{SF}) in the effective properties of RVEs with 12 fibres with respect to the RVE model with single fibre.

Model	E_1	E_2	E_3	G_{12}	G_{13}	G_{23}	ν_{12}	ν_{13}	ν_{23}
RVE 1	0.98	8.13	6.95	4.01	-2.28	-16.36	-1.31	0.67	-19.91
RVE 2	0.62	6.11	6.88	-4.44	0.72	-14.74	0.52	-0.71	-18.71
RVE 3	0.74	5.06	5.59	-7.71	-3.46	-14.24	0.44	-0.40	-15.51

Table 9

Percentage change (φ_{EXP}) in the effective properties of RVEs with 12 fibres with respect to the experimental result [16].

Model	E_1	E_2	G_{12}	G_{23}	ν_{12}	ν_{23}
RVE 1	-0.14	20.27	17.88	9.13	8.71	22.30
RVE 2	-0.51	18.52	10.65	10.40	10.36	23.08
RVE 3	-0.39	17.60	7.86	10.78	10.29	25.15

considered from experimental studies carried out in Soden et al. [16]. It must be noted that the properties of fibre are obtained by suitable micromechanics relations from lamina properties. The experimental value of the effective transverse shear modulus, G_{23} is obtained from effective transverse modulus, E_2 and through thickness Poisson's ratio, ν_{23} . Owing to lack of standardisation of experiments on composites and difficulties in measurements, variations in properties are expected from

Table 10

Effective properties of RVE model with twenty fibres (see Fig. 14).

Model	E_1 (GPa)	E_2 (GPa)	E_3 (GPa)	G_{12} (GPa)	G_{13} (GPa)	G_{23} (GPa)	ν_{12}	ν_{13}	ν_{23}
RVE 1	139.23	8.83	8.84	5.02	5.10	3.69	0.25	0.25	0.32
RVE 2	139.42	9.13	9.21	4.97	5.22	3.52	0.25	0.25	0.29
RVE 3	139.45	9.08	9.12	4.94	5.04	3.54	0.25	0.25	0.29
RVE 4	139.45	9.11	9.23	4.90	5.20	3.51	0.25	0.25	0.29
(μ)	139.39	9.04	9.11	4.96	5.17	3.57	0.25	0.25	0.30
(σ)	0.11	0.14	0.18	0.05	0.11	0.09	0.00	0.00	0.01
(ζ)	0.08	1.55	1.98	1.01	2.13	2.52	0.00	0.00	3.33

different experimental sources.

Predicted effective elastic constants for the RVE with single fibre (of circular cross section) are given in Table 5. The experimental results are

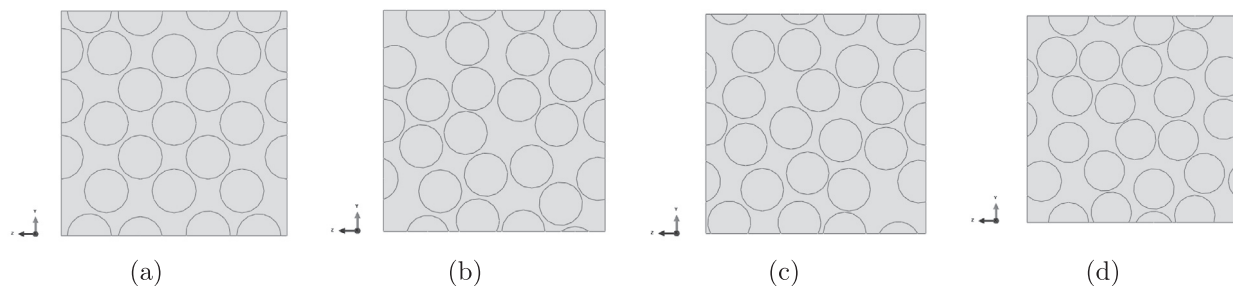


Fig. 14. Representative volume elements with 20 fibres. (a) RVE 1, (b) RVE 2, (c) RVE 3 and (d) RVE 4.

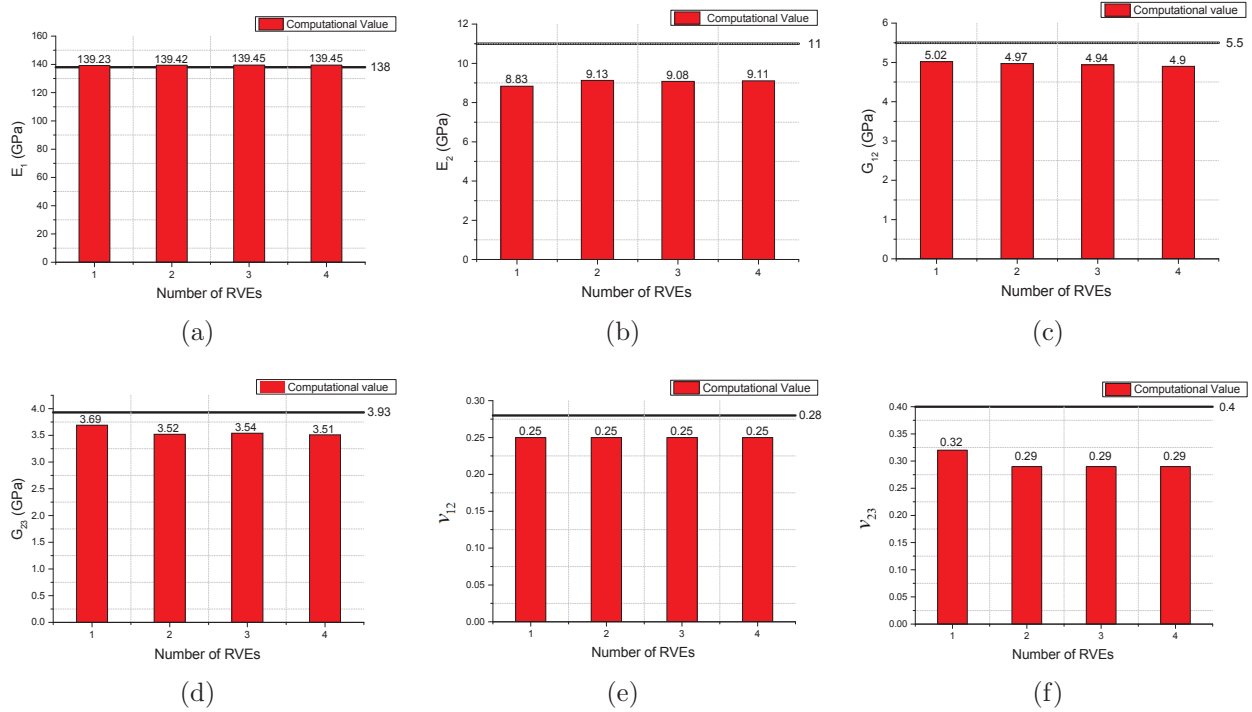


Fig. 15. Elastic constants with respect to experimental values for RVE with 20 fibres (a) Longitudinal modulus E_1 , (b) Transverse modulus E_2 , (c) Inplane shear modulus G_{12} , (d) Transverse shear modulus G_{23} , (e) Inplane Poisson's ratio ν_{12} , (f) Transverse Poisson's ratio ν_{23} .

Table 11

Percentage change (φ_{SF}) in the effective properties of RVEs with 20 fibres with respect to the RVE model with single fibre.

Model	E_1	E_2	E_3	G_{12}	G_{13}	G_{23}	ν_{12}	ν_{13}	ν_{23}
RVE 1	0.25	7.49	7.32	-6.74	-8.54	-20.39	0.40	0.63	-21.57
RVE 2	0.12	4.28	3.47	-5.68	-11.07	-14.74	-0.32	0.91	-11.30
RVE 3	0.09	4.86	4.38	-5.16	-7.27	-15.49	-0.16	0.59	-13.43
RVE 4	0.09	4.47	3.29	-4.34	-12.26	-14.39	-0.63	1.19	-11.11

Table 12

Percentage change (φ_{EXP}) in the effective properties of RVEs with 20 fibres with respect to the experimental result [16].

Model	E_1	E_2	G_{12}	G_{23}	ν_{12}	ν_{23}
RVE 1	-0.89	19.72	8.69	5.98	10.25	21.23
RVE 2	-1.03	16.93	9.59	10.39	9.61	27.88
RVE 3	-1.05	17.43	10.03	9.81	9.75	26.50
RVE 4	-1.05	17.09	10.74	10.66	9.32	28.00

given in Table 6. The predicted results are in agreement with experimental results. Homogenization method shows good prediction of the axial Young's modulus and in plane shear modulus, that is E_1 and G_{12} are very close to the experimental values. It is assumed that a unidirectional fibre-reinforced lamina is treated as transversely isotropic lamina and so the elastic constants are $E_1, E_2 = E_3, G_{12} = G_{13}$ and G_{23} . The typical percentage difference of the effective elastic constants are -1.14% for E_1 , 13.21% for E_2 and E_3 , 14.45% for G_{12} and G_{13} , 21.91% for G_{23} and 35.20% for ν_{23} with respect to the experimental results. The percentage difference/change (φ_{EXP}) with respect to experimental result is given by

$$\varphi_{EXP} = \left(\frac{E_i^{(EXP)} - E_i^{(RVE)}}{E_i^{(EXP)}} \right) * 100 \tag{15}$$

where $E_i^{(EXP)}$ generically refers to the experimental values and $E_i^{(RVE)}$ is for that particular RVE. However, the percentage difference/change (φ_{SF}) with respect to RVE with single fibre is given by

$$\varphi_{SF} = \left(\frac{E_i^{(SF)} - E_i^{(RVE)}}{E_i^{(SF)}} \right) * 100 \tag{16}$$

where $E_i^{(SF)}$ generically refers to RVE with single fibre. The % error (ζ) is calculated by considering the mean (μ) and standard deviation (σ) which is given as

$$\zeta = \left(\frac{\sigma}{\mu} \right) * 100$$

Here, the percentage difference in properties with respect to that of RVE with single fibre is reported because these are the most popularly reported properties in literature.

5.2. Case II: RVE with twelve fibres

Following the procedure of generating the RVE, we refined our analysis with random distribution of fibres maintaining the fibre volume fraction of 0.6. RVE with 12 fibres are shown in Fig. 12 with approximate dimension of $(3.97d \times 3.97d \times 3.97d)$. These RVEs are meshed with approximately 2,00,000 elements and 40,000 nodes, respectively. Here, the effect of randomness in fibre distribution on effective elastic properties is studied.

Observations are made for the predicted effective elastic constants of RVEs with fibres randomly distributed. Here, three RVE models considered are RVE 1, RVE 2 and RVE 3 as shown in Fig. 12. The predicted effective elastic coefficients are given in Table 7. As RVEs are modeled with random arrangements of fibre, there is a variation in

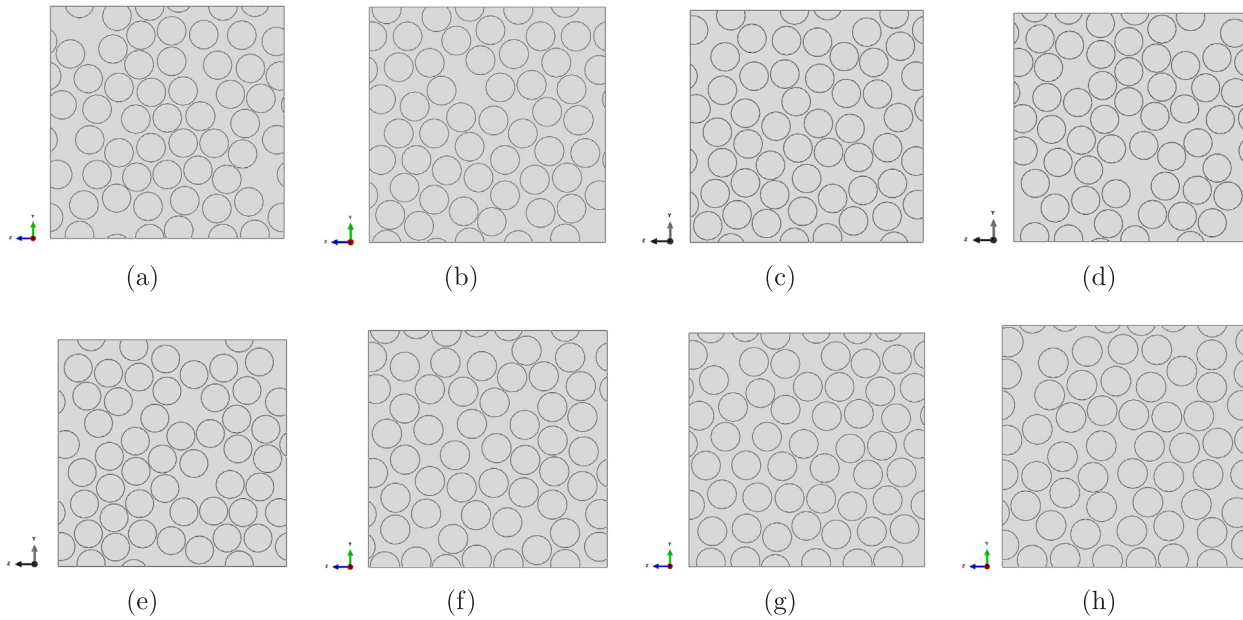


Fig. 16. Representative volume elements with 50 fibres of circular cross-sections. (a) RVE 1, (b) RVE 2, (c) RVE 3, (d) RVE 4, (e) RVE 5, (f) RVE 6, (g) RVE 7 and (h) RVE 8.

Table 13

Effective properties of RVE models with fifty fibres of circular cross-section (see Fig. 16).

Model	E_1 (GPa)	E_2 (GPa)	E_3 (GPa)	G_{12} (GPa)	G_{13} (GPa)	G_{23} (GPa)	ν_{12}	ν_{13}	ν_{23}
RVE 1	136.19	9.20	9.28	4.93	5.20	3.53	0.25	0.25	0.28
RVE 2	136.01	9.10	9.14	5.01	5.16	3.61	0.25	0.25	0.29
RVE 3	136.04	9.20	9.24	4.24	5.05	3.57	0.25	0.25	0.28
RVE 4	136.73	9.27	9.26	5.45	5.41	3.60	0.25	0.25	0.28
RVE 5	136.64	9.25	9.28	5.41	5.44	3.59	0.25	0.25	0.28
RVE 6	136.47	9.22	9.21	5.43	5.40	3.59	0.25	0.25	0.29
RVE 7	136.44	9.21	9.16	5.36	5.29	3.60	0.25	0.25	0.29
RVE 8	136.60	9.31	9.26	5.45	5.29	3.56	0.25	0.25	0.28
(μ)	136.39	9.22	9.23	5.17	5.28	3.59	0.25	0.25	0.28
(σ)	0.28	0.06	0.05	0.43	0.14	0.02	0.00	0.00	0.01
(ζ)	0.21	0.65	0.54	8.32	2.65	0.56	0.00	0.00	3.52

effective properties E_2 and E_3 in RVE 2 and RVE 3 as compared to RVE 1. This is as expected because for RVE 1 the fibres are more uniformly distributed, whereas for the other two RVEs they are randomly arranged (see Fig. 12). The standard deviation (σ) values for all the properties are less than 1 but (ζ) is more for G_{12} and ν_{23} , i.e. 5.8% and 10.34%, respectively and for the other properties it is less than 2% as given in Table 7. However, the mean (μ) values of all the constants are equal to or less than the experimental values reported in [16]. The comparison is shown in Fig. 13. The experimental results are shown as a reference line.

The percentage differences (φ_{SF}) between the properties obtained from the three RVEs are given in Table 8. Axial modulus, E_1 predicted for all the three RVEs with different fibre arrangement has percentage change less than 1% with respect to the effective properties of RVE with single fibre. However, for the transverse shear modulus, G_{23} , (φ_{SF}) the change is much higher compared to axial shear modulus G_{12} and G_{13} and is about 15%. Similarly, (φ_{SF}) can be as high as 19% for the transverse Poisson's ratio ν_{23} . This is due to the arrangement of fibres in the yz plane.

From Fig. 12, it can be noticed that most of the projected areas near the edges of the RVE are occupied by the fibres, this is the reason for the higher value of G_{23} . Table 9 shows the percentage change (φ_{EXP}) in the

effective properties with respect to the experimental results. It is noticed that (φ_{EXP}) for ν_{23} is much higher compared to the other properties which is almost 23%. From this, we can say that ν_{23} is significantly affected due to the random distribution of fibres.

5.3. Case III: RVE with twenty fibres

For this section, we consider the RVE of approximate dimensions ($5.15d \times 5.15d \times 5.15d$). The number of fibres are 20 in this RVE. The fibres are randomly distributed maintaining the volume fraction 0.6. Here, four RVE models are considered with different fibre arrangements as shown in Fig. 14. These RVEs are meshed with approximately 2,50,000 elements and 45,000 nodes, respectively. The predicted effective properties are tabulated in Table 10.

Table 10 shows the estimated effective properties, the average (μ) and standard deviation (σ). Also, (φ_{SF}) is estimated for this case. These are also compared with experimental values and are shown in Fig. 15. The mean (μ) values of all the properties are less than the experimental values, except for E_1 which is very close to experimental value as shown in Fig. 15(a). The standard deviation (σ) values for the RVEs with 20 fibres are less than one. Further, (ζ) is less than 1% for E_1 but for G_{13} , G_{23} and ν_{23} these are about 2–3%.

It is observed that (μ) of the elastic properties of RVE models with 20 fibres is higher comparable to RVE with 12 fibres. This is mainly due to increase in the number of fibres and also arrangement of the fibres. Increase in number of fibres by keeping the size of the RVE and fibre volume fraction constant, makes the RVE more stiffer. For this reason the values are higher compared to RVE with 12 fibres.

Axial modulus, E_1 predicted from all the four RVEs with different fibre arrangement has (φ_{SF}) less than 1% as given in Table 11. For RVE 1, (φ_{SF}) is more compared to the other three RVE models. This is mainly due to the fact that in RVE 1 the fibres are arranged in a uniform manner throughout the RVE. (φ_{SF}) for transverse shear modulus, G_{23} is much more for RVE 1 compared to other three RVE models due to the same reason as mentioned for RVE with 12 fibres.

Also from Fig. 14 it can be noticed that except RVE 1, the other three RVEs have some matrix rich regions which also affect the properties. Table 12 shows the percentage change (φ_{EXP}) of the effective properties with respect to the experimental values. It is observed that on comparison with experimental data, (φ_{EXP}) for E_1 is less than 1.2%.

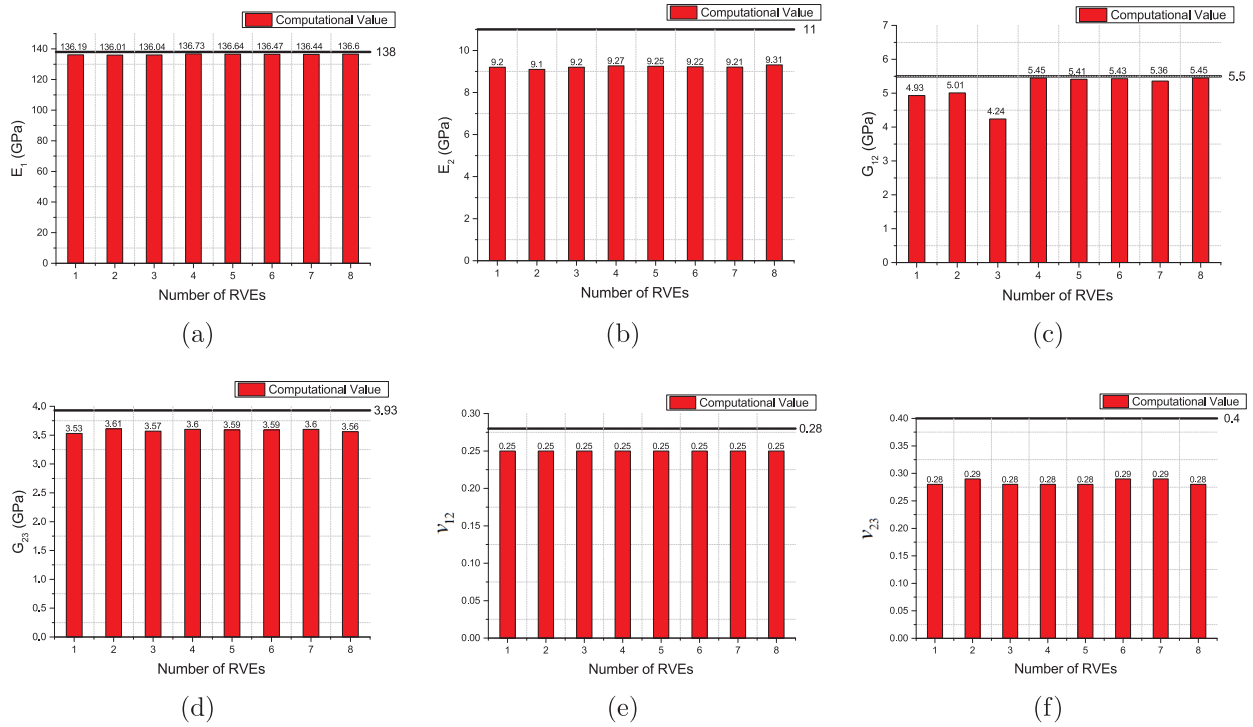


Fig. 17. Elastic constants with respect to the experimental values for RVEs with 50 fibres of circular cross-section (a) Longitudinal modulus E_1 , (b) Transverse modulus E_2 , (c) Inplane shear modulus G_{12} , (d) Transverse shear modulus G_{23} , (e) Inplane Poisson’s ratio ν_{12} , (f) Transverse Poisson’s ratio ν_{23} .

Table 14

Percentage change (φ_{SF}) in the effective properties of the RVEs with 50 fibres of circular cross section with respect to the RVE model with single fibre.

Model	E_1	E_2	E_3	G_{12}	G_{13}	G_{23}	ν_{12}	ν_{13}	ν_{23}
RVE 1	2.42	3.60	2.77	-4.93	-10.52	-15.34	-0.44	0.79	-9.03
RVE 2	2.56	4.66	4.22	-6.68	-9.66	-17.75	-0.16	0.52	-12.81
RVE 3	2.53	3.60	3.16	9.78	-7.46	-16.58	-0.16	0.52	-9.76
RVE 4	2.04	2.86	2.93	-16.01	-15.03	-17.46	0.52	0.39	-8.76
RVE 5	2.10	3.02	2.74	-15.10	-15.78	-17.19	0.36	0.52	-8.45
RVE 6	2.22	3.32	3.43	-15.57	-14.79	-17.03	0.44	0.28	-10.19
RVE 7	2.25	3.51	4.01	-14.03	-12.43	-17.31	0.59	-0.04	-11.11
RVE 8	2.13	2.40	2.96	-16.01	-12.49	-16.02	0.91	-0.24	-8.37

Table 15

Percentage change (φ_{EXP}) in the effective properties of RVEs with 50 fibres of circular cross section with respect to the experimental result [16].

Model	E_1	E_2	G_{12}	G_{23}	ν_{12}	ν_{23}
RVE 1	1.31	16.34	10.23	9.93	9.50	29.35
RVE 2	1.44	17.25	8.74	8.04	9.75	26.90
RVE 3	1.41	16.34	22.82	8.96	9.75	28.88
RVE 4	0.92	15.69	0.75	8.27	10.36	29.53
RVE 5	0.99	15.83	1.53	8.48	10.21	29.73
RVE 6	1.11	16.10	1.13	8.61	10.29	28.60
RVE 7	1.13	16.26	2.45	8.39	10.43	28.00
RVE 8	1.01	15.30	0.76	9.39	10.71	29.78

However, for ν_{23} it is much higher and approximately 26%. Even from Fig. 15 it is noticed that for ν_{23} the variation is much more compared to the experimental data. Thus, ν_{23} has a significant effect due to random fibre distribution.

5.4. Case IV: RVE with fifty fibres

In this section, the variation in the fibre cross-section with the effect of randomness has also been discussed and their effects on the effective properties are studied. Here, RVEs with 50 fibres maintaining the same





RVE size and the volume fraction 0.6 are generated but with different fibre arrangements shown in Fig. 16. Here, RVEs with the variation in fibre cross-section are modeled maintaining the centres of the fibres at the same position inside the RVE domain for the circular, distorted and elliptical cross-sections.

5.4.1. RVE with fibres of circular cross sections

Here, eight different RVEs are modeled to study the clustering effect of fibres on the effective properties. These RVEs are shown in Fig. 16 and their effective properties are given in Table 13. These RVEs are meshed with approximately 5,50,000 elements and 1,00,000 nodes, respectively.

Observations are made for these RVEs for the effect of randomness in fibre arrangement. When we increase the number of fibres to 50, it is noticed that there is a reduction in effective axial modulus, E_1 with respect to the RVE with single fibre, 12 and 20 fibres but there is a little increment in the mean (μ) values of other effective properties. (σ) values in the properties for these RVEs are less than 1. Further, (ζ) is less than 1% except for G_{12} , G_{13} and ν_{23} which are equal to 8.32%, 2.65% and 3.52%, respectively. The comparison of these properties with respect to the experimental values are shown in Fig. 17. It can be seen that predicted values of E_1 and G_{12} are in comparison with experimental results. However, for the other properties there is a significant

Table 16
Variation of σ_{RMS} along the depth of RVEs with circular fibre cross section for different load cases.

	$(\epsilon_{(0),xx})$	$(\epsilon_{(0),yy})$	$(\epsilon_{(0),zz})$	$(\epsilon_{(0),yz})$	$(\epsilon_{(0),xz})$	$(\epsilon_{(0),xy})$
 Periodic Arrang.	1.36E04	1.93E04	1.35E04	1.96E04	1.85E05	1.44E05
 RVE 1	1.88E04	1.10E04	8.27E03	8.71E03	2.91E04	3.38E04
 RVE 2	1.59E04	9.99E03	8.27E03	9.11E03	3.18E04	3.02E04
 RVE 3	8.86E02	1.01E04	8.54E03	9.34E03	2.45E04	2.33E04
 RVE 4	1.29E04	4.69E04	3.47E04	2.77E04	2.03E05	2.06E05
 RVE 5	1.20E04	3.84E04	2.54E04	2.94E04	1.92E05	1.94E05
 RVE 6	1.10E05	4.86E04	3.06E04	2.82E04	2.34E05	2.15E05
 RVE 7	2.31E05	4.19E04	3.37E04	2.95E04	2.04E05	1.99E05
 RVE 8	3.52E04	4.13E04	2.98E04	2.90E04	2.22E05	1.98E05
(μ)	5.46E04	3.10E04	2.25E04	2.14E04	1.42E05	1.37E05
(σ)	7.91E04	1.74E04	1.19E04	1.02E04	9.53E04	9.00E04
(ζ)	144.89	56.12	52.90	47.80	66.87	65.46

difference. For E_1 , (φ_{EXP}) is less than 1.5% for all the RVEs whereas for G_{12} , except RVE 1, 2 and 3 (φ_{EXP}) is less than 3%. However, for the other properties it is within a range between (8 and 30)%.

The percentage change (φ_{SF}) is reported in Table 14. It can be seen that (φ_{SF}) for all the properties is more than 1%. The change is approximately 4% for longitudinal and transverse moduli but for shear moduli it varies between 4 and 17%. Except RVE 1, 2 and 3 (φ_{SF}) is more than 12%. Further, (φ_{SF}) of effective transverse moduli E_2 and E_3 are reduced compared to RVE with 12 and 20 fibres. Table 15 shows the percentage change (φ_{EXP}) in the effective properties with respect to the experimental result. It is observed that (φ_{EXP}) for E_1 is less than 1.5%

however, for ν_{23} it is very high, i.e. approximately 28%. For RVE 3, it is noticed that G_{12} has very high (φ_{EXP}), i.e. 22% compared to other RVE models.

After studying the variation of the effective properties due to random fibre arrangements, we have extended the study to the variation of RMS value of the micro stresses, σ_{RMS} due to unit macro strains. In this study, the effect of macro normal and shear strains are considered for both periodic and random arrangements of fibres with circular cross section. Table 16 presents the σ_{RMS} for RVEs with circular fibre cross section for both periodic and random fibre arrangements.

From Table 16 it is clearly seen that σ_{RMS} values are significantly higher for macro shear strain cases compared to the macro normal strain cases. The highest value of σ_{RMS} is for RVE 7 for macro strain $\epsilon_{(0),xx}$ (2.31E05). This makes the percentage error for macro strain $\epsilon_{(0),xx}$ very large, i.e. 144.89%. From Table 16 it can be noticed that (ζ) is within the range of (50–65)% except for $\epsilon_{(0),xx}$ and $\epsilon_{(0),yz}$ which are 114.89% and 47.80%, respectively. Further, contour plots for the variation of σ_{RMS} on the plane perpendicular to the fibre direction are shown in Fig. 18 and Fig. 19. Fig. 18 shows the variation of σ_{RMS} for the periodic arrangement of fibres and Fig. 19 shows the variation of σ_{RMS} for random fibre distribution of circular fibre cross section. These plots also show the areas of high stress concentration.

Fig. 18(a), (b), (c) are for the macro normal strains and (d), (e), (f) are for macro shear strains. However, for both the cases the variation of σ_{RMS} is in a periodic manner and also they show the regions of high stress concentration where the damage initiation is expected to take place. When the fibres are periodically arranged it is noticed from the contour plots that the high concentration regions also occurred in a periodic manner depending on the applied load case.

However, for Fig. 19 where the fibres are randomly distributed, the scenarios are different. Here, the fibres are of circular cross section and are randomly arranged in the RVEs. There are some fibre-rich regions, i.e. the fibres are very close to each other and also there are matrix rich regions, i.e. where there are no fibres present.

Further, contour plots for the variation of σ_{RMS} in an RVE with random fibre distributions are shown in Fig. 19. Interestingly, for Fig. 19 (a) the values are much less compared to the other plots as it is for macro strain $\epsilon_{(0),xx}$ where the loading is along the fibre direction. However, for the other load cases the variation of σ_{RMS} is very prominent. The areas of high stress concentration regions are easily identified and they depend on different regions inside the RVE and the applied load cases. It mainly occurs for the regions where the fibres are very close to each other, i.e. fibre rich regions. It can also be concluded that these are the regions which are highly prone to damage initiation. Eventually, the highest value of σ_{RMS} occurs for macro strain $\epsilon_{(0),xz}$ which is 2.620E04 for this particular fibre arrangement. This doesn't mean that for all the arrangements σ_{RMS} will be the highest for $\epsilon_{(0),xz}$, it depends on the arrangement of fibres. Thus, random fibre distribution/arrangement plays a vital role in the variation of σ_{RMS} .

5.4.2. RVE with fibres of distorted cross sections

Here, RVEs with distorted fibre cross sections are studied. The fibres are randomly distributed as shown in Fig. 20. The volume fractions for these RVEs are less compared to those of the circular cross section as the fibres have distorted cross sections. This plays a vital role which reflects in the estimation of effective properties. Here, eight RVE samples are studied for the effect of randomness and distortion of fibre cross section on the effective properties. They are meshed with approximately 6,50,000 elements and 1,30,000 nodes, respectively.

The effective properties for these RVEs are given in Table 17 and the percentage change (φ_{SF}) is given in Table 18. From Table 17 it is observed that Young's modulus E_1 shows a significant reduction in comparison with circular fibre cross section. However, for other properties there is not much of change. The change in Young's modulus E_1 is mainly due to the reduction in volume fraction as the fibres are distorted. (ζ) is less than 1% for axial, transverse moduli and G_{23} . However,

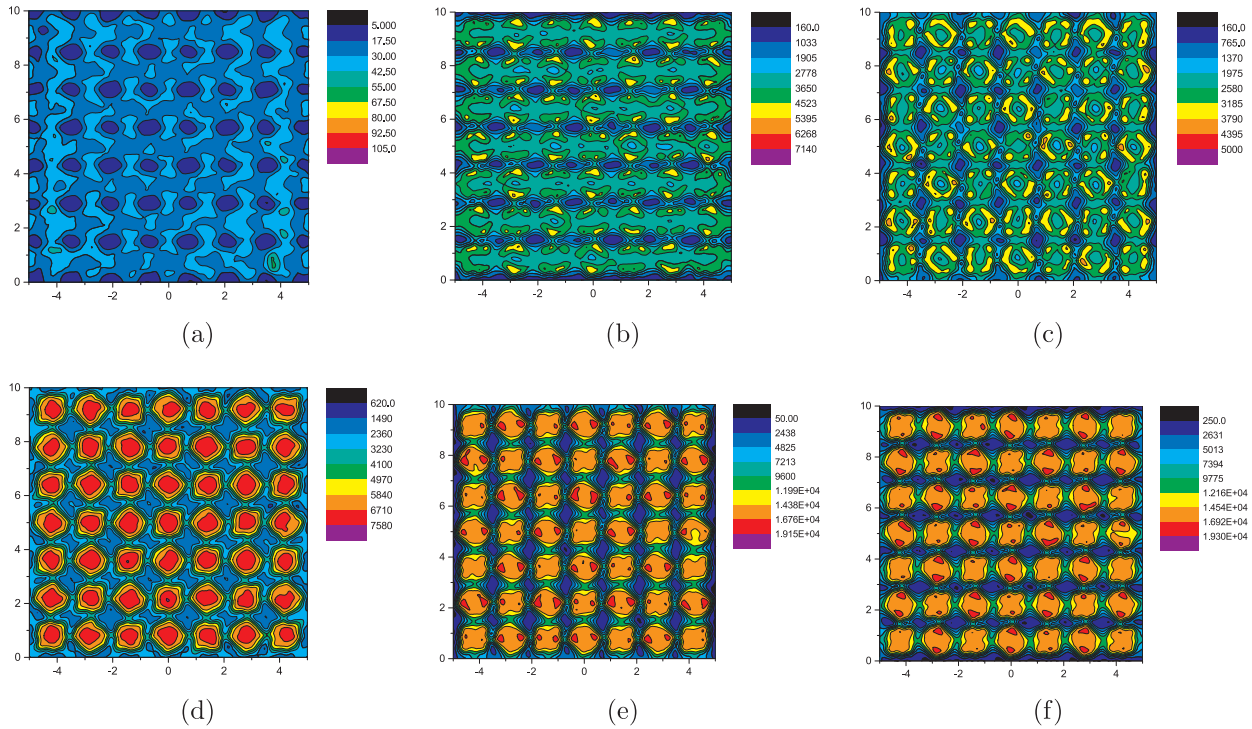


Fig. 18. Variation of σ_{RMS} of RVE with periodic arrangement (circular fibre cross section) for different load cases. (a) Macro strain ($\epsilon_{(0),xx}$), (b) macro strain ($\epsilon_{(0),yy}$), (c) macro strain ($\epsilon_{(0),zz}$), (d) macro strain ($\epsilon_{(0),yz}$), (e) macro strain ($\epsilon_{(0),xz}$) and (f) macro strain ($\epsilon_{(0),xy}$).

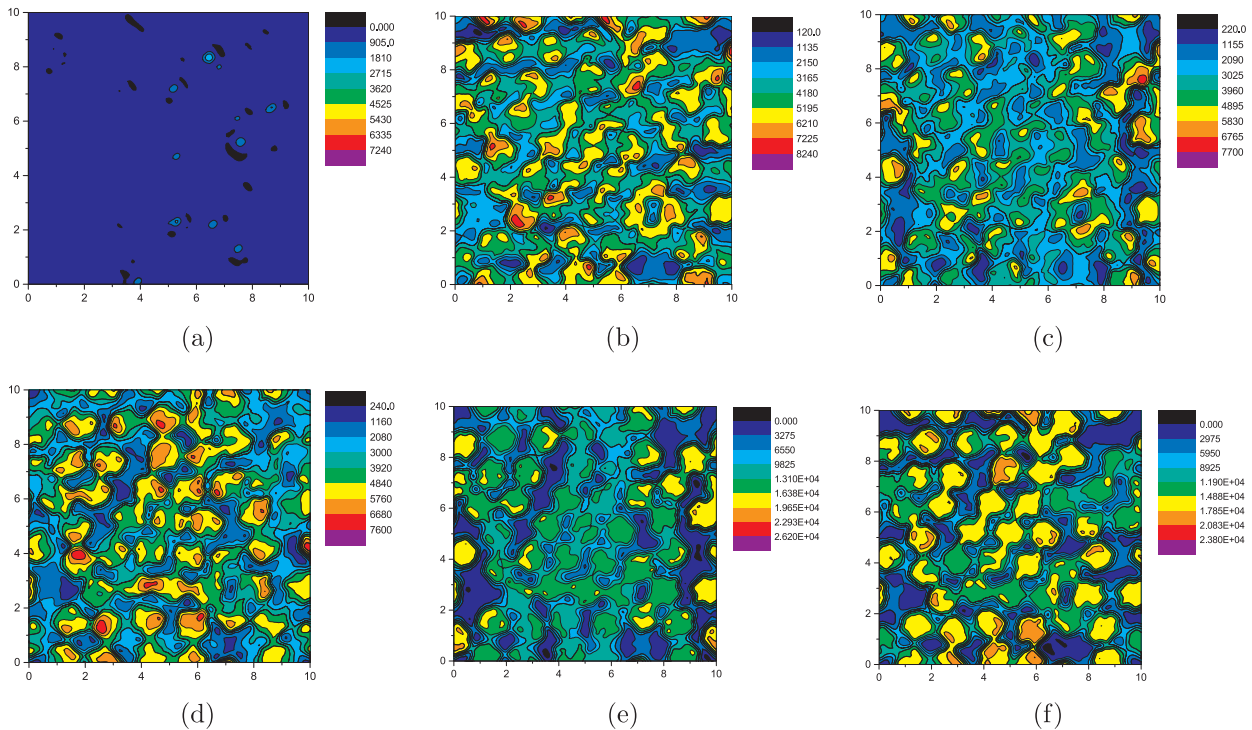


Fig. 19. Variation of σ_{RMS} in an RVE with random arrangement (RVE 1 – circular fibre cross section) for different load cases. (a) macro strain ($\epsilon_{(0),xx}$), (b) macro strain ($\epsilon_{(0),yy}$), (c) macro strain ($\epsilon_{(0),zz}$), (d) macro strain ($\epsilon_{(0),yz}$), (e) macro strain ($\epsilon_{(0),xz}$) and (f) macro strain ($\epsilon_{(0),xy}$).

for G_{12} and G_{13} it is about 3.02% and 2.30% (see Table 17). (σ) for all the properties are less than 1, that means the effective properties do not have a severe effect due to distortion of fibres.

However, errors in the effective properties with respect to the experimental values are shown in Fig. 21. It is observed that for the effective properties E_2 and ν_{23} the variation is much more compared to

the other effective properties with respect to the experimental results.

From Table 18, it is observed that the values of E_1 , E_2 and E_3 show about 7% change. Similarly, this change for G_{12} is about - 18% and for G_{13} and G_{23} it is about - 14% when compared to that of RVE with single fibre. (φ_{SF}) of shear moduli G_{13} and G_{23} for RVE 3 is much less compared to other RVE models because more number of fibres are concentrated at

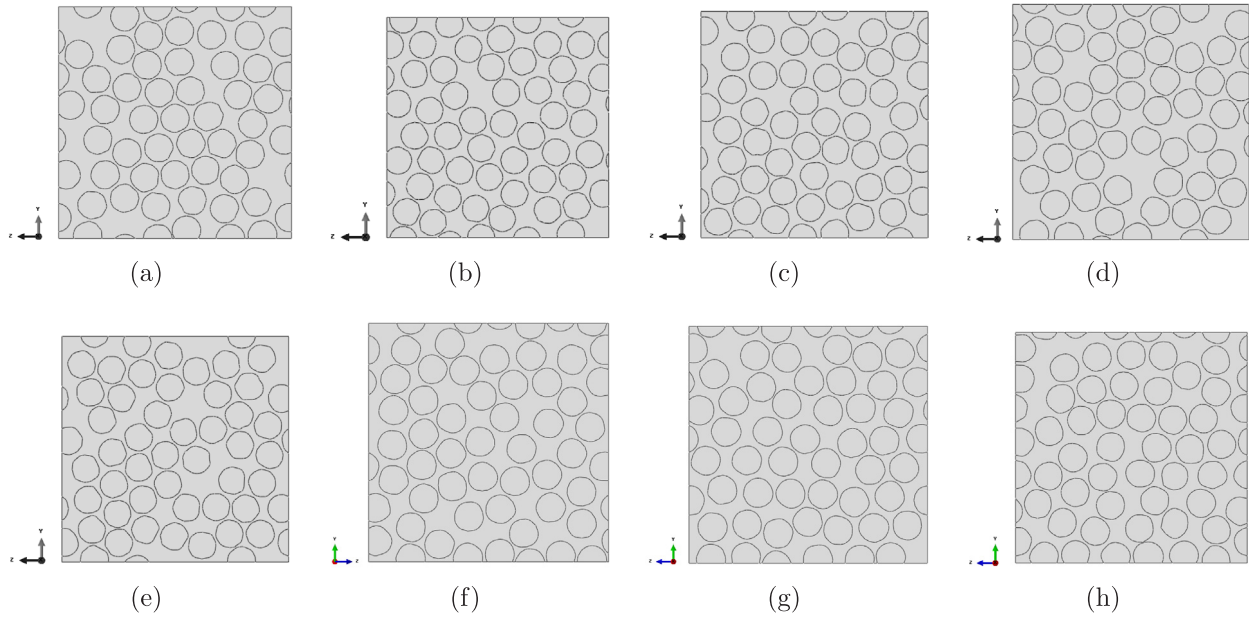


Fig. 20. Representative volume elements with 50 fibres of distorted cross-section. (a) RVE 1, (b) RVE 2, (c) RVE 3, (d) RVE 4, (e) RVE 5, (f) RVE 6, (g) RVE 7 and (h) RVE 8.

Table 17
Effective properties of RVE models with fifty fibres of distorted cross-section (see Fig. 20).

Model	E_1 (GPa)	E_2 (GPa)	E_3 (GPa)	G_{12} (GPa)	G_{13} (GPa)	G_{23} (GPa)	ν_{12}	ν_{13}	ν_{23}
RVE 1	132.18	9.12	9.07	5.41	5.28	3.50	0.25	0.25	0.29
RVE 2	131.63	8.96	8.89	5.24	5.11	3.53	0.25	0.26	0.30
RVE 3	131.48	8.97	9.00	5.02	5.07	3.47	0.25	0.25	0.29
RVE 4	130.91	8.99	8.98	5.22	5.17	3.46	0.25	0.25	0.29
RVE 5	130.11	8.95	8.95	5.21	5.15	3.43	0.25	0.26	0.29
RVE 6	131.48	8.99	8.99	5.33	5.33	3.47	0.25	0.25	0.29
RVE 7	130.65	8.95	8.91	5.30	5.21	3.47	0.25	0.26	0.30
RVE 8	131.79	9.13	9.08	5.55	5.41	3.49	0.25	0.25	0.29
(μ)	131.28	9.01	8.99	5.29	5.22	3.48	0.25	0.25	0.29
(σ)	0.68	0.07	0.07	0.16	0.12	0.03	0.00	0.00	0.00
(ζ)	0.52	0.78	0.78	3.02	2.30	0.86	0.00	0.00	0.00

the centre of the RVE.

Further, Table 19 shows the percentage change (φ_{EXP}). (φ_{SF}) is less than 6% for E_1 and G_{12} but for E_2 and ν_{23} it is almost 18% and 26%, respectively. So from experimental point of view E_2 and ν_{23} have significant effect due to fibre cross section and also due to their random distribution.

Here, we studied the variation of RMS value of the micro stresses σ_{RMS} due to unit macro strains. However here the fibres are of distorted cross section. The effect of macro normal and shear strains are considered. Table 20 presents the σ_{RMS} for RVEs with distorted fibre cross

Table 18
Percentage change (φ_{SF}) in the effective properties of the RVEs with 50 fibres of distorted cross section with respect to the RVE model with single fibre.

Model	E_1	E_2	E_3	G_{12}	G_{13}	G_{23}	ν_{12}	ν_{13}	ν_{23}
RVE 1	5.29	4.44	4.96	-15.06	-12.37	-14.09	-0.08	-0.83	-11.19
RVE 2	5.69	6.14	6.79	-11.47	-8.77	-15.27	-0.24	-1.07	-15.93
RVE 3	5.79	5.97	5.70	-6.75	-7.89	-13.38	-1.03	-0.67	-13.12
RVE 4	6.21	5.79	5.91	-10.99	-9.94	-13.03	-0.87	-0.99	-13.19
RVE 5	6.78	6.18	6.21	-10.85	-9.55	-12.06	-0.99	-1.19	-13.54
RVE 6	5.79	5.76	5.82	-13.44	-13.29	-13.26	-0.87	-0.87	-13.62
RVE 7	6.39	6.23	6.65	-12.77	-10.84	-13.33	-0.67	-1.35	-15.01
RVE 8	5.58	4.35	4.83	-18.08	-15.12	-13.86	0.12	-0.91	-11.19

section.

From Table 20 it is noticed that σ_{RMS} values are in the same range for both normal and shear macro strain cases, unlike for fibres with circular fibre cross section where we observe higher values for shear strain cases compared to normal strain cases. (ζ) for $\epsilon_{(0),yy}$ is only 7.83% compared to other macro strain which is almost or above 50% except for $\epsilon_{(0),xy}$ which is 27.25% (see Table 20). On noticing (σ) value, the value for $\epsilon_{(0),xx}$ is higher compared to other macro strain cases which is $3.15E05$ thus we can say $\epsilon_{(0),xx}$ has significant effect on the variation of σ_{RMS} for this particular fibre arrangement.

Further contour plots for the variation of σ_{RMS} over the RVEs with distorted fibre cross section are shown in Fig. 22. These plots show the regions of high stress concentration due to applied macro strains of different types. It is also observed that the maximum stress value occurs for macro strain $\epsilon_{(0),yy}$, $\epsilon_{(0),xz}$ and $\epsilon_{(0),xy}$ for this particular fibre arrangement. So from these contour plots we can say the failure or initiation of damage will occur mostly at the fibre rich regions irrespective of the applied load cases.

5.4.3. RVE with fibres of elliptical cross sections

RVEs with elliptical fibre cross sections are considered and are randomly distributed. RVEs are modeled with elliptical fibre cross-section with +0.5% of the radius of the circular fibre cross-section as major axis and -0.5% of the circular fibre cross-section as minor axis as shown in Fig. 23. The fibres are evenly distributed across the window with random orientations, i.e. the major axis of the elliptical fibre cross-section is placed randomly in the y-z plane. Here also we have

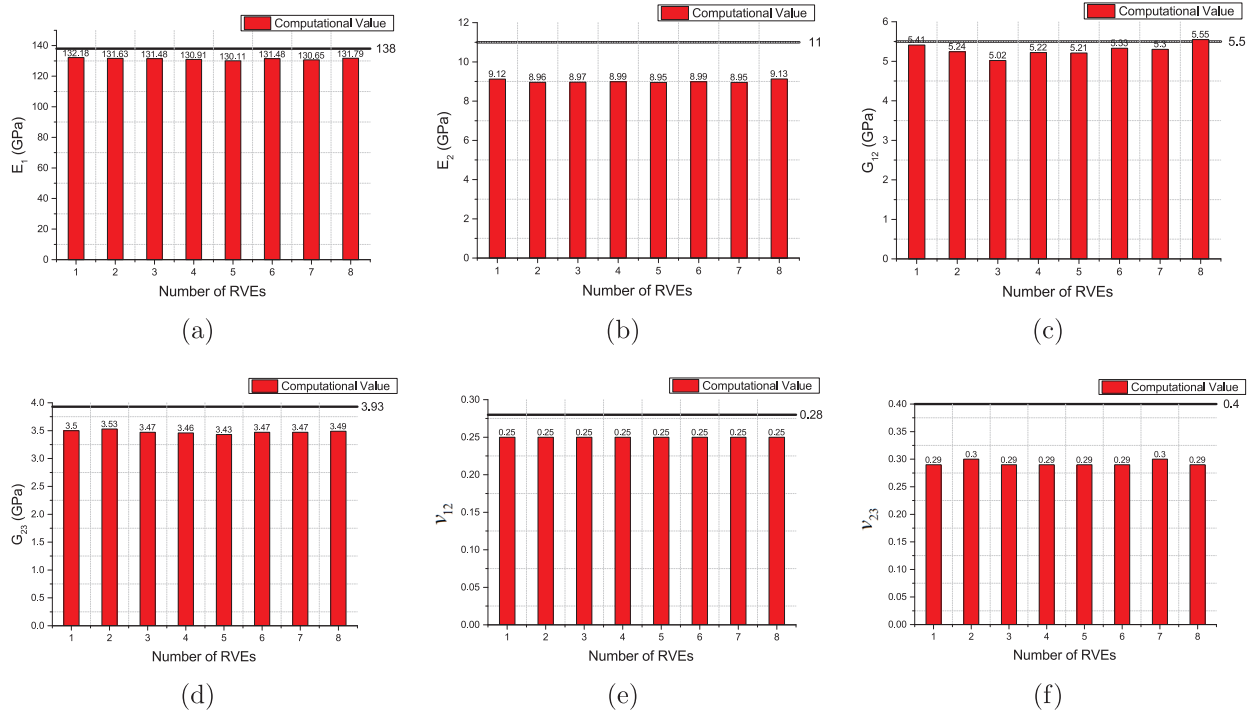


Fig. 21. Elastic properties with respect to experimental value with 50 fibres of distorted cross-section. (a) Longitudinal modulus E_1 , (b) Transverse modulus E_2 , (c) Inplane shear modulus G_{12} , (d) Transverse shear modulus G_{23} , (e) Inplane Poisson's ratio ν_{12} , (f) Transverse Poisson's ratio ν_{23} .

Table 19

Percentage change (φ_{EXP}) is in the effective properties of RVEs with 50 fibres of distorted cross section with respect to the experimental result [16].

Model	E_1	E_2	G_{12}	G_{23}	ν_{12}	ν_{23}
RVE 1	4.21	17.07	1.56	10.90	9.82	27.95
RVE 2	4.61	18.54	4.63	9.89	9.68	24.88
RVE 3	4.72	18.39	8.68	11.46	8.96	26.70
RVE 4	5.14	18.25	5.04	11.73	9.11	26.65
RVE 5	5.72	18.58	5.17	12.49	9.00	26.43
RVE 6	4.72	18.21	2.95	11.52	9.11	26.38
RVE 7	5.32	18.62	3.52	11.50	9.29	25.48
RVE 8	4.50	16.99	-1.02	11.08	10.00	27.95

considered eight RVE samples and studied how the randomness of fibre arrangement with elliptical fibre cross sections affect the variation in effective properties. These RVEs are meshed with approximately 5,75,000 elements and 1,20,000 nodes, respectively.

The effective properties for the RVEs with elliptical fibre cross section are tabulated in Table 21. The effective property values are very close to the RVEs of circular cross section. The standard deviation (σ) for all the properties are less than 1 and (ζ) is also less than 1, except for G_{12} and G_{13} and it is about 2.6% and 2.06%, respectively. Thus, we can say randomness with elliptical fibre cross section has negligible effect on the effective properties. In Fig. 24, the error in the elastic constants with respect to the experimental results are shown. It is noticed that the computation results of E_1 and G_{12} are almost matching with the experimental results. However, there is a large variation with the experimental results for E_2 and ν_{12} (see Fig. 24).

The percentage change (φ_{SF}) is given in Table 22. (φ_{SF}) for E_1 is about 2.6%, whereas for E_2 and E_3 it is about 4.5%. (φ_{SF}) for shear moduli is varying between (12 and 18)%.

The percentage change (φ_{EXP}) is shown in Table 23. It is noticed that (φ_{EXP}) for E_1 is less than 1.5% for all the RVE models, however for E_2 is about 16%. It is observed that not only E_2 has high percentage change but also for ν_{23} which is about 29%. Thus, with respect to experimental results, E_2 and ν_{23} have a significant effect for this particular fibre

arrangement of elliptical fibre cross section.

From the study carried out in this section it can be understood that with increase in the number of fibres in the RVE, the obtained properties converge and approach the experimental values. However, some transverse properties can be up to 30% different from the experimental values.

Remark on the goodness of the computational results: It is noticed that the transverse properties E_2 and ν_{23} do not match well with the experimental results. On considering the computed values obtained for the RVEs of 50 fibres with circular cross sections it is observed that E_2 shows a variance of up to 17% with respect to the experimental results. It is noticed that experimental data for E_2 is 11 GPa and computational data for E_2 is 9.22 GPa. However, % error in E_2 is $[(11 - 9.22)/11] * 100 = 16.18\%$. If we carry out a simple standard mechanics analysis with E_2 of fibre of 15 GPa [16] then E_2 (of composite) as

$$\frac{1}{E_2} = \left(\frac{V_f}{E_f^{(f)}} + \frac{V_m}{E^{(m)}} \right) = \left(\frac{0.6}{15} + \frac{0.4}{4.2} \right) \Rightarrow E_2 = 7.3948$$

Now assuming a pathological case of waviness, i.e the fibre is locally turned by 90° , we get

$$\frac{1}{E_2} = \left(\frac{V_f}{E_f^{(f)}} + \frac{V_m}{E^{(m)}} \right) = \left(\frac{0.6}{225} + \frac{0.4}{4.2} \right) \Rightarrow E_2 = 10.214$$

Both these results are not close to desired experimental value of 11. This points to a need to take a relook at the experimental result itself. From these it can be said that this is best that can be done in micro mechanics considering the realistic situations about fibre cross section and distributions. A similar analysis can be applied for ν_{23} . Further, the variation in fibre cross sectional geometry does not have much effect on effective properties. But, it can significantly effect stress distribution which plays an important role in damage initiation and its propagation. Finally, the variation of σ_{RMS} due to unit macro strains for elliptical fibre cross section is studied. In this study, the effect of macro normal and shear strains are considered on random arrangements of fibres.

Table 20
Variation of σ_{RMS} along the depth of RVEs with distorted fibre cross section for different load cases.


	$(\epsilon_{(0),xx})$	$(\epsilon_{(0),yy})$	$(\epsilon_{(0),zz})$	$(\epsilon_{(0),yz})$	$(\epsilon_{(0),xz})$	$(\epsilon_{(0),xy})$
 RVE 1	2.45E05	5.30E04	1.01E05	8.29E04	6.45E05	2.55E05
 RVE 2	3.03E05	4.88E04	3.92E04	3.34E04	1.95E05	1.89E05
 RVE 3	2.52E05	5.08E04	3.18E04	2.62E04	2.12E05	1.90E05
 RVE 4	3.34E05	4.34E04	3.84E04	2.97E04	2.03E05	1.95E05
 RVE 5	2.47E05	4.71E04	3.34E04	3.15E04	2.22E05	1.89E05
 RVE 6	1.52E05	5.65E04	3.67E04	3.07E04	3.50E05	3.25E05
 RVE 7	2.89E05	4.87E04	3.79E04	3.39E04	2.28E05	2.43E05
 RVE 8	1.14E06	5.04E04	4.00E04	3.68E04	3.16E05	3.56E05
	3.70E05	4.98E04	4.48E04	3.81E04	2.96E05	2.43E05
(μ)	3.15E05	3.90E03	2.30E04	1.84E04	1.52E05	6.61E04
(σ)	85.06	7.83	51.25	48.16	51.17	27.25
(ζ)						

Table 24 presents the σ_{RMS} for RVEs with elliptical fibre cross section.

From **Table 24** it is observed that (ζ) of σ_{RMS} for macro strain $\epsilon_{(0),xx}$ is very high of 101.34% compared to other macro strains which are in the range of (11–18)%. However, (σ) is more for macro strain $\epsilon_{(0),xx}$, i.e. 1.12E05 compared to other macro strains. Further, contour plots for the variation of σ_{RMS} over the RVEs with elliptical fibre cross section are shown in **Fig. 25**. These plots show the regions of high stress concentration due to applied macro strains of different types.

From the contour plots, it is observed that the maximum σ_{RMS} value occurs for macro strain $\epsilon_{(0),yy}$, $\epsilon_{(0),xz}$ and $\epsilon_{(0),xy}$. Even from the contour plots of macro shear strains there are many areas/zones which are highly prone to failure or initiation of damage. For some load cases it occurs near the edges of the RVE or at the fibre rich regions (where the

fibres are very close to each other). So from the damage initiation point of view, randomness plays a vital role as in some scenarios fibre arrangements sometimes restrict the initiation of damage as the fibres are sitting on the path of the initiation of damage.

5.5. Master RVE

In this study, the effect of the variation in the local volume fraction on the effective elastic properties at different positions inside the RVE due to the random distribution of the fibres is noticed. Here, two RVE models are considered. In the first RVE model, we fixed the window size and then this window is moved throughout the RVE to estimate the effective properties. In the second RVE model, different sizes of the window are considered and they are moved throughout the RVE to estimate the effective properties. Here, the notion of homogenization convergence has been studied to eliminate the geometrical periodicity requirement when the size of RVE is sufficiently large. The numerical studies realize the multiscale nature of the convergence of overall material properties as the unit cell size is increased. Here, initially the master RVE of dimension approximately $(1.1442d)$, where d is the diameter of the fibre, is modeled with cubic domain and periodicity. To analyze the local behaviour or to do a detailed analysis of the composite, we sectioned the master RVE into a number of sub samples called super frames.

5.5.1. Model RVE 1

For the model RVE 1, the master RVE domain was divided into 16 equal cuboidal domains as shown in **Fig. 26**. The boundaries of the super frames intersect the fibres but the connectivity between the super frames is maintained. Here, three cases studied are: estimation of effective properties (i) for single super frame, (ii) combination of 4 super frames and (iii) combination of 9 super frames. Finally, the percentage change of each super frame is compared with the whole RVE model. In Case (i) Model, a single RVE of 50 fibres is modeled into 16 windows of single super frame and named as A to P. These are shown in **Fig. 26**. It can be seen that some of the super frames have fibre rich regions while some of them are matrix rich regions and due to this there is a variation in the fibre volume fraction in each super frame.

The effects of variation of volume fraction, matrix and fibre rich regions and also the randomness in the fibre distribution on effective properties are studied. We start the analysis by solving the master domain problem with displacement boundary conditions for all the six load cases and estimate the effective elastic properties.

Case (i): Here, single super frames are considered for this study as shown in **Fig. 27**. On account of single super frame, sixteen windows/super frames are generated for the study of the effective properties. Here, the window A has low fibre volume fraction as it is mostly composed of matrix rich region. Also there are other windows with fibre rich regions.

The results for effective properties of individual windows are given in **Table 25**. It can be seen that the fibre volume fraction varies from 37% to 75%. For windows A to P, it can be seen that the window A has matrix rich region with fibre volume fraction of 37%. The Young's modulus, E_1 is 88.12 GPa, which is much less compared to values for other windows. This is obviously due to lesser fibre volume fraction. However, for Window B and G, the fibre volume fraction is much more, i.e. 75.08% and 73.82%, respectively and considered as a fibre rich region as fibres are more clustered. For these two windows the effective axial modulus is 173.84 GPa and 171.01 GPa, respectively which is much more compared to other windows. It is noticed that for Windows C to F and H to P, there is a variation in fibre volume fraction from 50.96% to 68.80%, due to which the effective axial modulus, E_1 varies from 116.43 GPa to 159.69 GPa. Thus, this study clearly brings out the fact that volume fraction plays a vital role on the effective properties. It has been noticed that the (μ) fibre volume fraction is 59.73% and for this the average value of E_1 is 139.15 GPa, which is very close to the

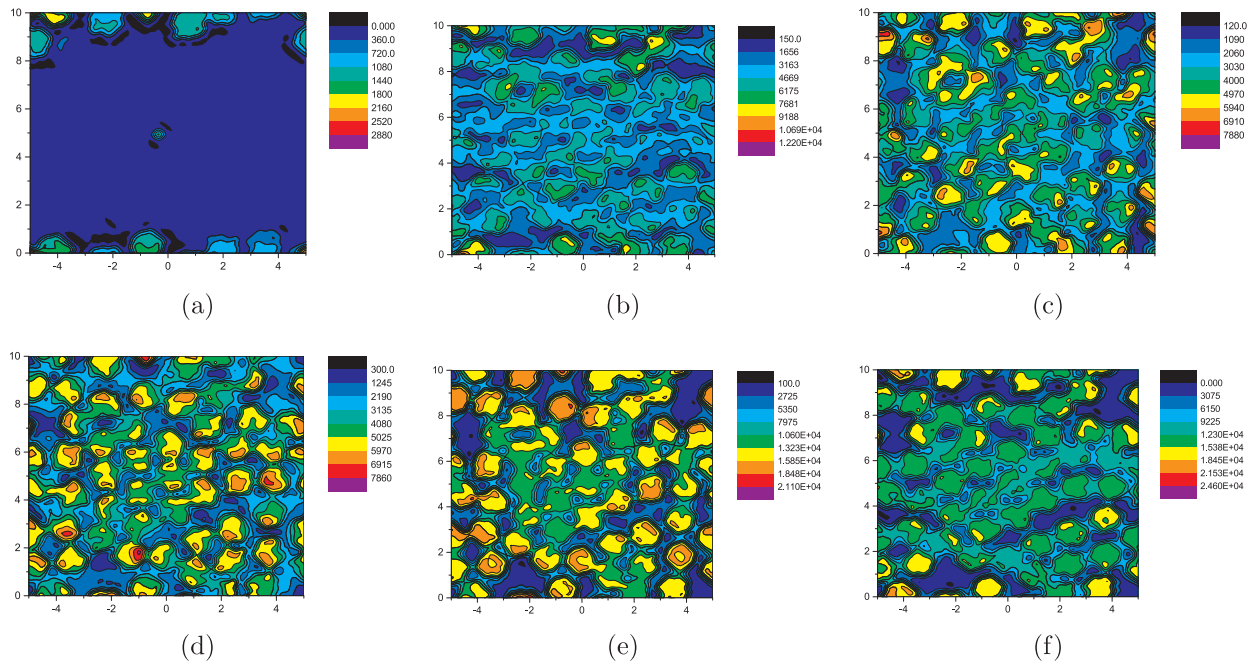


Fig. 22. Variation of σ_{RMS} of RVE with random arrangement (RVE 1 – distorted fibre cross section) for different loadcases (a) macro strain $(\epsilon_{(0),xx})$, (b) macro strain $(\epsilon_{(0),yy})$, (c) macro strain $(\epsilon_{(0),zz})$, (d) macro strain $(\epsilon_{(0),yz})$, (e) macro strain $(\epsilon_{(0),xz})$ and (f) macro strain $(\epsilon_{(0),xy})$.

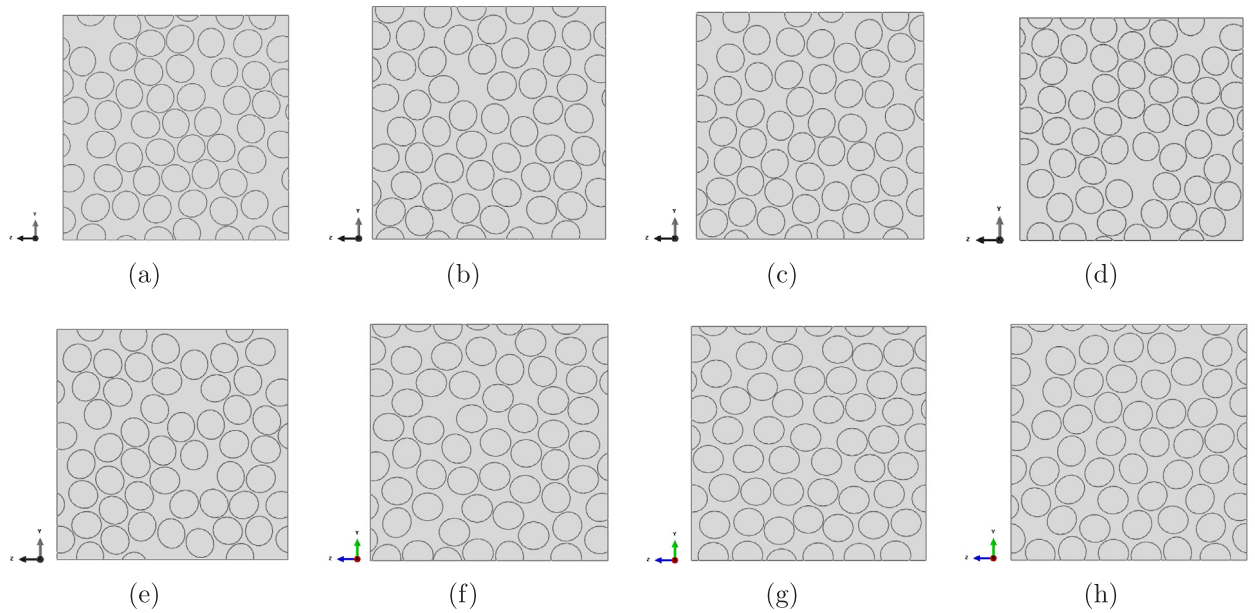


Fig. 23. Representative volume elements with 50 fibres of elliptical cross-section. (a) RVE 1, (b) RVE 2, (c) RVE 3, (d) RVE 4, (e) RVE 5, (f) RVE 6, (g) RVE 7 and (h) RVE 8.

experimental value. However, all the other (μ) effective property values are more than the experimental values. For all the super frames, i.e from window A to P (σ) is less than 2.2 for all the (μ) effective properties except for E_1 which is about 22.49. This means the longitudinal modulus, E_1 significantly depends on the local volume fraction and the random distribution of the fibres.

In Case (ii) combination of 4 super frames are considered for this study as shown in Fig. 28(a)–(d). On account of combination of 4 super frames, 9 RVE models are generated for the study of effective properties. The first 4 sets of RVEs are modeled at the four corners of master RVE. And the other RVEs are modeled at the edges and centre of the master RVE as shown in Fig. 28(e)–(i). Observations are made for the prediction of elastic constants of these RVEs with the effect of local

volume fraction. The effective properties are reported in Table 26. For these combinations of super frames the fibre volume fraction varies from 55% to 67%. The fibre volume fraction for window HIOP is about 55.91% which is the lowest of all the windows and for this window the Young’s modulus, E_1 is 130.65 GPa. On the contrary, it is noticed that for window CFGH, E_1 is 155.69 GPa as the fibre volume fraction is about 67.02%. Thus, fibre rich or matrix rich regions play a vital role in prediction of effective properties.

In addition to the (μ) values, the standard deviations (σ) of all the super-frames with different combinations are estimated. (σ) for all the RVEs with different combination of windows are less than 1, except for E_1 which is 7.63. This is as expected because the E_1 is dominated by the volume fraction. Thus, the variation in volume fraction reflects directly

Table 21
Effective properties of RVE models with fifty fibres of elliptical cross-section (see Fig. 23).

Model	E_1 (GPa)	E_2 (GPa)	E_3 (GPa)	G_{12} (GPa)	G_{13} (GPa)	G_{23} (GPa)	ν_{12}	ν_{13}	ν_{23}
RVE 1	135.94	9.26	9.19	5.52	5.31	3.57	0.25	0.25	0.28
RVE 2	135.94	9.15	9.09	5.48	5.29	3.62	0.25	0.25	0.29
RVE 3	136.31	9.21	9.23	5.27	5.23	3.58	0.25	0.25	0.28
RVE 4	136.39	9.26	9.22	5.50	5.29	3.59	0.25	0.25	0.28
RVE 5	136.48	9.27	9.27	5.41	5.34	3.58	0.25	0.25	0.28
RVE 6	135.91	9.16	9.19	5.27	5.42	3.58	0.25	0.25	0.29
RVE 7	135.93	9.18	9.28	5.12	5.58	3.55	0.25	0.25	0.28
RVE 8	135.93	9.26	9.25	5.35	5.31	3.54	0.25	0.25	0.28
(μ)	136.11	9.22	9.22	5.37	5.35	3.58	0.25	0.25	0.28
(σ)	0.24	0.05	0.06	0.14	0.11	0.03	0.00	0.00	0.00
(ζ)	0.18	0.54	0.65	2.61	2.06	0.84	0.00	0.00	0.00

in the variation of E_1 . However, (ζ) is less than 6% for all the effective properties.

In Case (iii) combination of 8 super frames are considered as shown in Fig. 29. On account of combination of 8 super frames, four model RVEs are generated for the study of effective properties. All the 4 sets of RVEs are modeled at the four corners of master RVE as shown in Fig. 29(a)–(d). Observations are made for the predicted elastic constants from these RVEs with the effect of local volume fraction. In addition to the (μ) values the standard deviations in the values of effective properties for all the super-frames with different combinations are calculated.

The predicted effective properties are given in Table 27 and the fibre volume fraction varies from 61% to 64% but the (μ) value is about 62.51% with (σ) of 1.28. The average values for all the properties are less than the experimental values. (σ) is less than 1 for all properties but for E_1 , it is 2.89. (ζ) is less than 3% for all the properties except for ν_{23} which is 6.37%.

5.5.2. Model RVE 2

This section is devoted to examine the effects of RVE size selection on the macroscopic mechanical behaviours of general heterogeneous media. Here, we divided another master RVE model into thirty-two subdivisions and estimated the effective properties. The RVE is shown in Fig. 30.

Here, the master RVE is sectioned into 32 combinations of more finer divisions compared to master Model RVE 1. It is divided unequally as shown in Fig. 30. For studying the effect of local volume fraction, square sections are considered as shown in Fig. 31. Here, three cases are considered: (i) windows at the interior of the master RVE, (ii) windows near the boundary edges of the master RVE and (iii) windows gradually increasing the size from interior of the master RVE to the full master RVE. It can be easily seen here that the super frames have fibre rich and matrix rich regions resulting in a variation of the fibre volume fraction in super frames. Here, it is studied that how this variation of volume fraction and randomness in the fibre arrangement affect the effective properties.

Case (i): Considering the windows/super frames at the interior of the master RVE, four RVEs are modeled as shown in Fig. 31. The results for their effective properties are given in Table 28. It can be seen that for these RVEs the fibre volume fraction varies from 50% to 64%. It is noticed that window AE is composed of less number of fibres and there is presence of matrix rich region as shown in Fig. 31(a). This can be also noticed from the Table 28. The super frame has volume fractions of 50.64%, which is less than other super frames. Due to low fibre volume fraction for window AE the effective property E_1 is also less, i.e. 118.76 GPa, compared to other RVEs.

For window DH and CG the fibre volume fraction is more compared to remaining four windows as these are the fibre rich regions. Due to this E_1 and E_2 have higher value compared to other windows. However, the (μ) values of all the effective properties are more compared to the experimental value as well as those of RVE with single fibre. This is mainly due to the effect of local fibre volume fraction and random arrangements of fibre distribution. (σ) is less than 2 for all the properties,

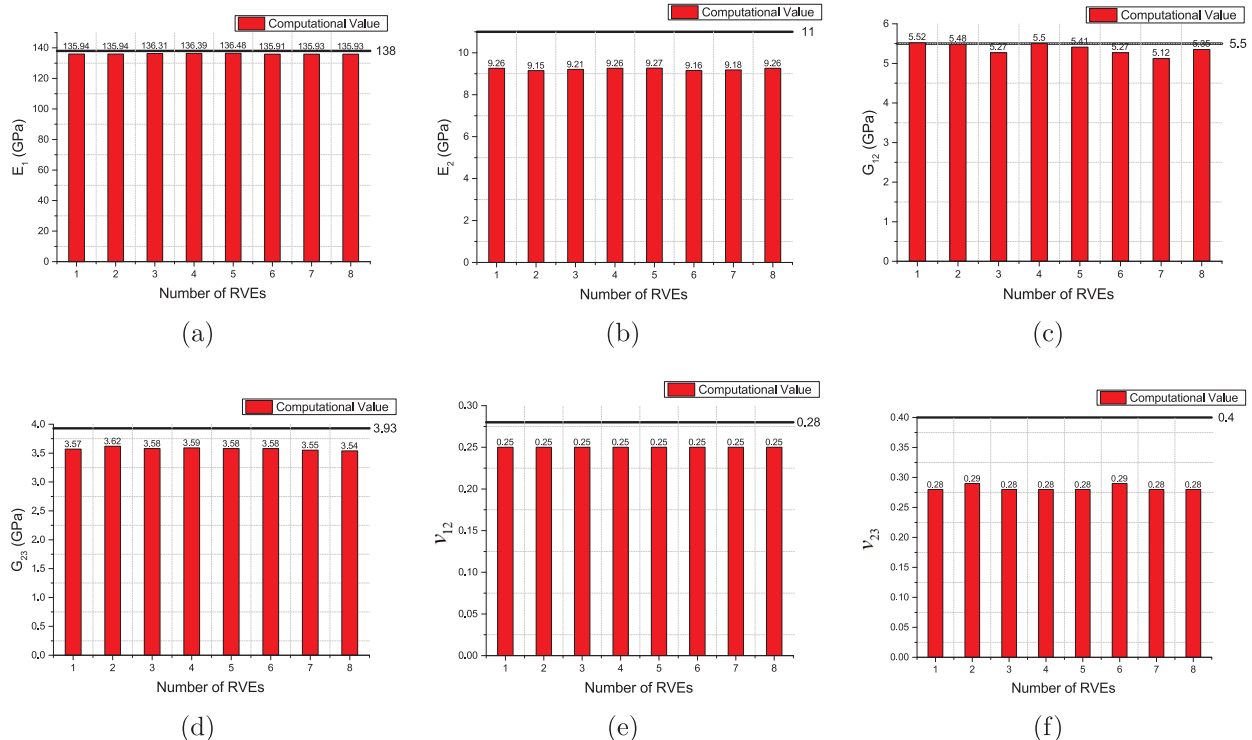


Fig. 24. Elastic constants with respect to experimental value with 50 fibres of elliptical cross-section. (a) Longitudinal modulus E_1 , (b) Transverse modulus E_2 , (c) Inplane shear modulus G_{12} , (d) Transverse shear modulus G_{23} , (e) Inplane Poisson's ratio ν_{12} , (f) Transverse Poisson's ratio ν_{23} .

Table 22

Percentage change (φ_{SP}) in the effective properties of the RVEs with 50 fibres (elliptical cross section) with respect to the RVE model with single fibre.

Model	E_1	E_2	E_3	G_{12}	G_{13}	G_{23}	ν_{12}	ν_{13}	ν_{23}
RVE 1	2.60	2.91	3.69	-17.45	-12.88	-16.41	0.83	-0.48	-9.72
RVE 2	2.60	4.13	4.74	-16.59	-12.62	-18.13	0.63	-0.20	-12.92
RVE 3	2.33	3.46	3.26	-12.13	-11.17	-16.90	0.28	0.28	-9.57
RVE 4	2.28	2.89	3.41	-17.04	-12.51	-17.25	0.75	-0.04	-9.57
RVE 5	2.21	2.81	2.87	-15.11	-13.60	-16.77	0.52	0.28	-8.64
RVE 6	2.62	4.02	3.63	-12.15	-15.27	-16.86	-0.12	0.48	-10.73
RVE 7	2.61	3.79	3.07	-8.87	-18.69	-15.69	-0.59	0.99	-8.68
RVE 8	2.61	2.97	3.07	-13.72	-12.84	-15.49	0.36	-0.08	-8.60

Table 23

Percentage change (φ_{EXP}) in the effective properties of RVEs with 50 fibres of elliptical cross section with respect to the experimental result [16].

Model	E_1	E_2	G_{12}	G_{23}	ν_{12}	ν_{23}
RVE 1	1.49	15.74	-0.48	9.09	10.64	28.90
RVE 2	1.49	16.80	0.25	7.75	10.46	26.83
RVE 3	1.22	16.22	4.07	8.71	10.14	29.00
RVE 4	1.17	15.73	-0.13	8.44	10.57	29.00
RVE 5	1.10	15.65	1.53	8.81	10.36	29.60
RVE 6	1.51	16.71	4.05	8.74	9.79	28.25
RVE 7	1.50	16.51	6.86	9.65	9.36	29.58
RVE 8	1.50	15.80	2.71	9.81	10.21	29.63

except E_1 which is 17.15. This means that E_1 is significantly affected by this fibre distribution and local fibre volume fraction effect.

Case (ii): Here, the windows/superframes near the boundary edges of the master RVE are considered. Four RVEs are modeled as shown in Fig. 32. The results for effective properties of these RVEs are given in Table 29. It can be seen that the fibre volume fraction varies from 57% to 64% and the mean (μ) fibre volume fraction is about 62.91%. The E_1 value for window AEIJT, as shown in Fig. 32 (a), is 134.84 GPa and much less than other RVE models as it has the presence of matrix rich region within this window. (σ) for E_1 is 8.27, which is much higher compared to the other effective properties. For other properties it is less than 1 as given in Table 29. (ζ) is approximately 6% for E_1 , E_2 and G_{12} whereas for the other properties it is less than 3%.

Case (iii): The windows/superframes with gradually increasing in the size from the interior of the master RVE to the full size of the master RVE are modeled as shown in Fig. 33. The results for their effective properties are reported in Table 30. Here, the fibre volume fraction varies from 58% to 62% with the increase in the window size maintaining the aspect ratio of the window to a constant.

The effective axial modulus, E_1 for the window ABCD is 137.17 GPa which is very close to the full RVE window, i.e. 139.10 GPa as the volume fractions are almost same for both the windows. (μ) value of the effective properties are higher than the experimental values and also RVE with single fibre. (σ) for E_1 is 3.99 but for the other properties it is less than 1. (ζ) for all the properties are less than 10% and from the Table 30 we can conclude that the longitudinal modulus, E_1 has significant effect due to the randomness and local volume fraction.

From this study it is clearly seen that by narrowing the window size for RVE the significant amount of variation in volume fraction is observed. As the window size is increased to the master RVE the volume fraction and the effective properties approaches to that of master RVE. Thus, the selection of RVE size for master RVE plays an important role. In this study the Young's modulus E_1 is significantly affected due to large variation in the volume fraction.

6. Conclusion

In the present study, a statistical representation of unidirectional fibre reinforced composite material at microscale through a representative volume element with random fibre distribution has been

Table 24

Variation of σ_{RMS} along the depth of RVEs with elliptical fibre cross section for different loadcases.

	$(\epsilon_{(0),xx})$	$(\epsilon_{(0),yy})$	$(\epsilon_{(0),zz})$	$(\epsilon_{(0),yz})$	$(\epsilon_{(0),xz})$	$(\epsilon_{(0),xy})$
 RVE 1	1.95E05	4.45E04	3.01E04	3.72E04	2.94E05	1.97E05
 RVE 2	2.04E04	4.96E04	3.15E04	3.11E04	1.86E05	2.11E05
 RVE 3	1.46E05	4.53E04	2.93E04	2.75E04	1.79E05	2.00E05
 RVE 4	1.11E04	4.13E04	3.54E04	3.23E04	2.07E05	2.02E05
 RVE 5	1.03E04	4.15E04	2.71E04	2.91E04	2.00E05	2.70E05
 RVE 6	1.79E05	3.74E04	2.96E04	2.61E04	2.36E05	2.03E05
 RVE 7	3.07E05	3.48E04	4.06E04	3.01E04	2.17E05	1.78E05
 RVE 8	1.79E04	4.05E04	2.67E04	2.67E04	1.87E05	2.35E05
(μ)	1.11E05	4.19E04	3.13E04	3.00E04	2.13E05	2.12E05
(σ)	1.12E05	4.66E03	4.63E03	3.63E03	3.74E04	2.83E04
(ζ)	101.34	11.12	14.80	12.08	17.54	13.34

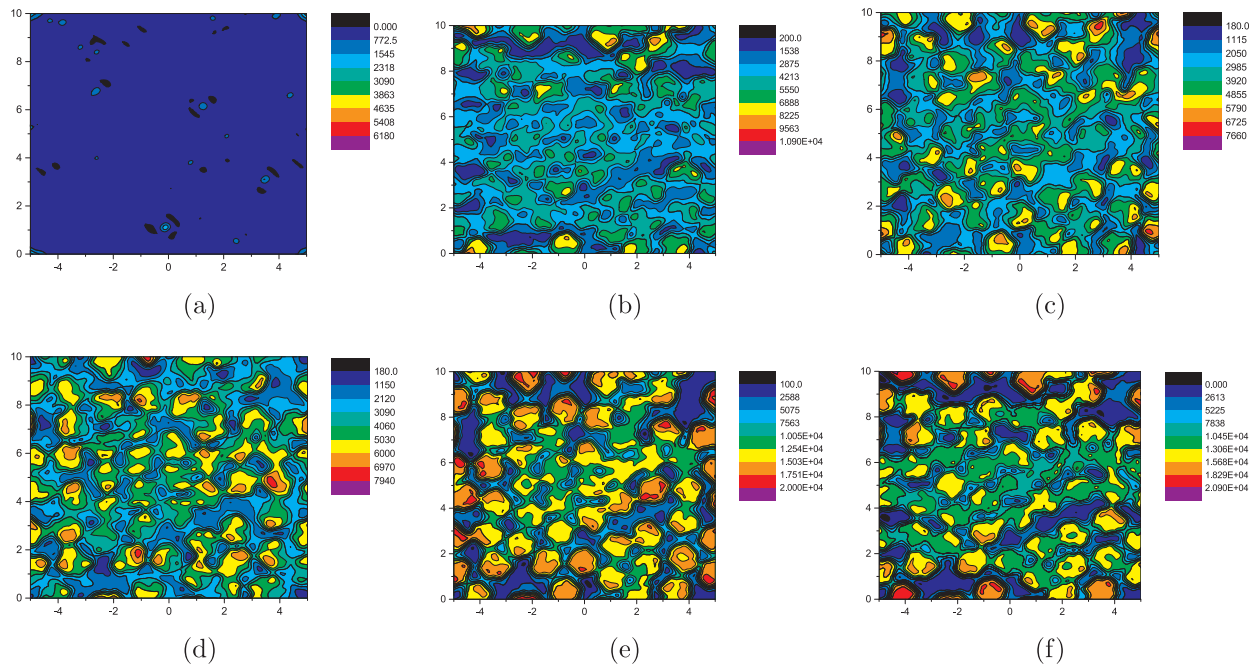


Fig. 25. Variation of σ_{RMS} of RVE with random arrangement (RVE 1 – elliptical fibre cross section) for different load cases. (a) Macro strain ($\epsilon_{(0),xx}$), (b) macro strain ($\epsilon_{(0),yy}$), (c) macro strain ($\epsilon_{(0),zz}$), (d) macro strain ($\epsilon_{(0),yz}$), (e) macro strain ($\epsilon_{(0),xz}$) and (f) macro strain ($\epsilon_{(0),xy}$).

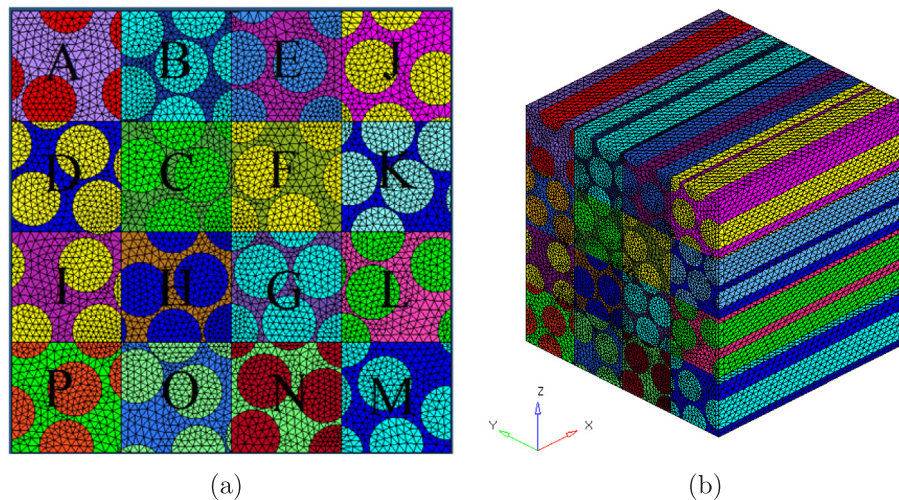


Fig. 26. Master RVE model 1. (a) Master RVE with different super-frames – front view, (b) Master RVE with different super-frames – isometric view.

developed. Image processing technique has been used to estimate the scatter, i.e. to estimate the fibre distribution. The fibre distribution in the composite microstructure SEM image has been considered to reconstruct the three dimensional RVE models. The modified algorithm using MATLAB has been proposed to generate statistically equivalent fibre distribution which is similar to the real scenario as the fibre distribution is obtained from a micrograph. Geometric periodicity is implemented while developing the RVE to ensure the continuity of the fibres across the neighbouring RVEs. Mathematical theory of homogenization has been implemented for the prediction of effective stiffness. The influence of spatial distribution of heterogeneities on the overall behaviour of the heterogeneous material has been investigated. Here, a comprehensive study is carried out to estimate the effective properties of RVEs having 1, 12, 20 and 50 fibres considering the effect of random fibre distribution. Further, RVEs with fibres randomly distributed in a periodic unit cell but with different fibre cross sections are modeled. Fibre waviness is not incorporated in this work, however it is

noticed [32] that the effect of waviness was not significant in RVE with single fibre. Finally, the effects of the variation in the local volume fraction on the effective elastic properties due to the random distribution of the fibres are also carried out. A good prediction of the inplane mechanical properties is achieved by using homogenization method with respect to experimental values. It is noticed that the effective property values obtained from three dimensional micromechanics are in good agreement with the experimental results taken from world wide failure exercise [17] except for E_2 and ν_{23} .

The major conclusions that can be drawn from this study are:

1. RVE with single fibre predicts inplane effective properties that are in good agreement with experimental results except E_2 which has a variance of 14%. Further for random RVE with fifty fibres the discrepancy remains. This difference may be outcome of the experimental process adopted to get E_2 , and hence needs to be looked at carefully.

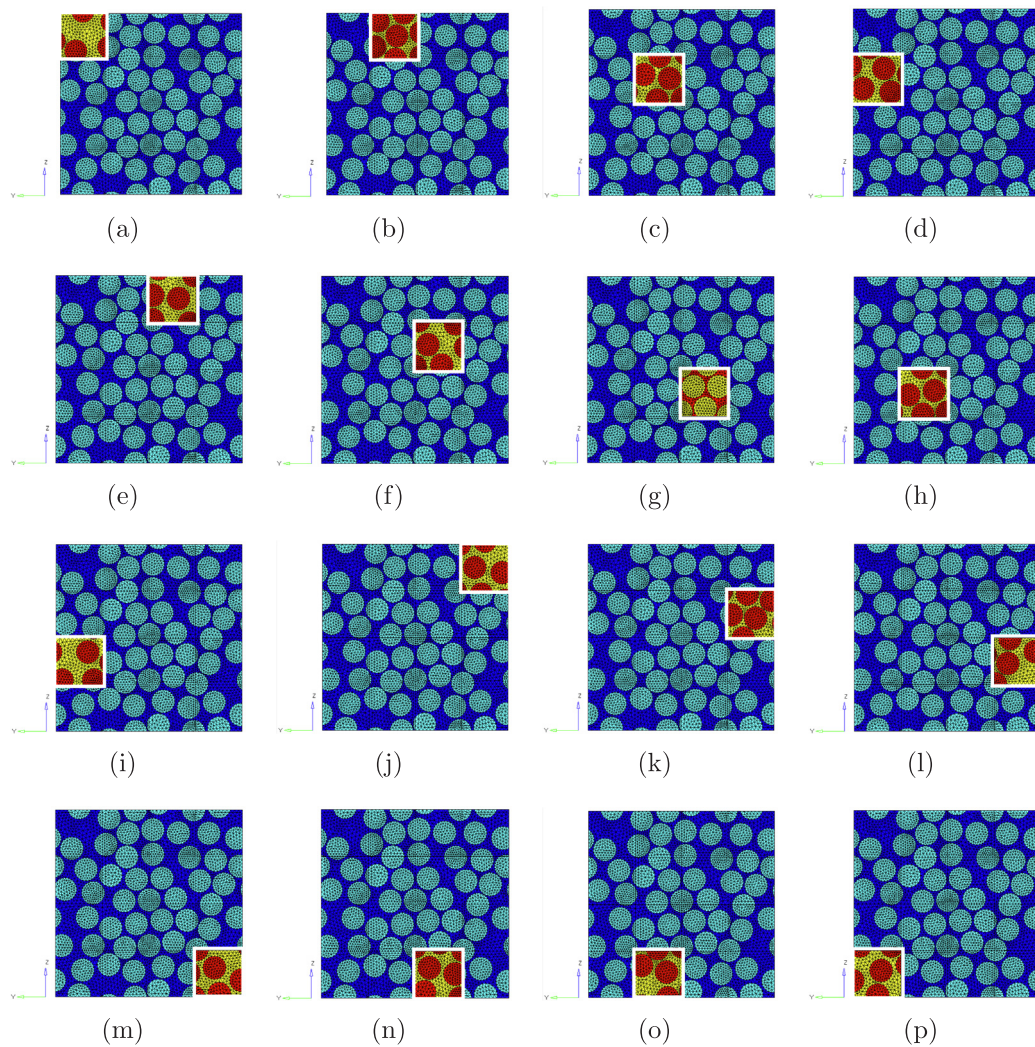


Fig. 27. RVEs with single superframes for master RVE - model 1. (a) Window A, (b) Window B, (c) Window C, (d) Window D, (e) Window E, (f) Window F, (g) Window G, (h) Window H, and (i) Window I, (j) Window J, (k) Window K, (l) Window L, (m) Window M, (n) Window N, and (o) Window O and (p) Window P.

Table 25
Effective properties of Master RVE with single super frame.

Window	Volume fraction		Effective properties								
	V_f	V_m	E_1 (GPa)	E_2 (GPa)	E_3 (GPa)	G_{12} (GPa)	G_{13} (GPa)	G_{23} (GPa)	ν_{12}	ν_{13}	ν_{23}
Window A	37.05	62.95	88.12	12.46	11.21	5.32	4.36	4.91	0.29	0.30	0.54
Window B	75.08	24.92	173.84	15.52	18.44	5.97	8.41	5.65	0.30	0.28	0.34
Window C	68.23	31.77	158.41	16.29	17.79	6.49	7.43	4.93	0.29	0.29	0.35
Window D	64.84	35.16	150.77	15.90	12.94	7.26	5.33	5.67	0.28	0.30	0.52
Window E	57.05	42.95	133.21	14.87	16.37	5.47	6.55	4.91	0.30	0.29	0.38
Window F	59.48	40.52	138.70	15.50	16.38	5.60	6.29	4.46	0.30	0.29	0.37
Window G	73.82	26.18	171.01	16.30	16.65	7.21	7.30	5.80	0.29	0.29	0.42
Window H	66.56	33.44	154.64	15.61	16.74	6.20	6.86	5.34	0.30	0.29	0.38
Window I	50.39	49.61	116.43	13.80	13.40	5.26	5.09	4.72	0.30	0.30	0.43
Window J	52.76	47.24	123.54	12.71	14.61	4.96	6.00	5.16	0.30	0.29	0.41
Window K	68.80	31.20	159.69	16.30	15.66	6.98	6.30	5.57	0.29	0.29	0.42
Window L	54.70	45.30	127.90	14.72	15.09	5.75	6.08	4.77	0.29	0.29	0.40
Window M	54.90	45.10	128.36	15.16	13.61	5.99	5.47	5.12	0.29	0.30	0.48
Window N	64.56	35.44	150.15	13.78	17.77	5.44	7.98	5.45	0.30	0.28	0.36
Window O	56.54	43.46	132.05	13.86	16.85	5.08	6.75	4.72	0.30	0.29	0.35
Window P	50.96	49.04	119.49	14.22	12.92	5.87	5.17	5.34	0.29	0.30	0.49
(μ)	59.73	40.27	139.15	14.82	15.41	5.93	6.34	5.16	0.29	0.29	0.42
(σ)	9.93	9.93	22.49	1.23	2.09	0.73	1.11	0.40	0.00	0.01	0.06
(ζ)	16.62	24.65	16.16	8.33	13.59	12.29	17.46	7.80	1.66	2.17	14.93

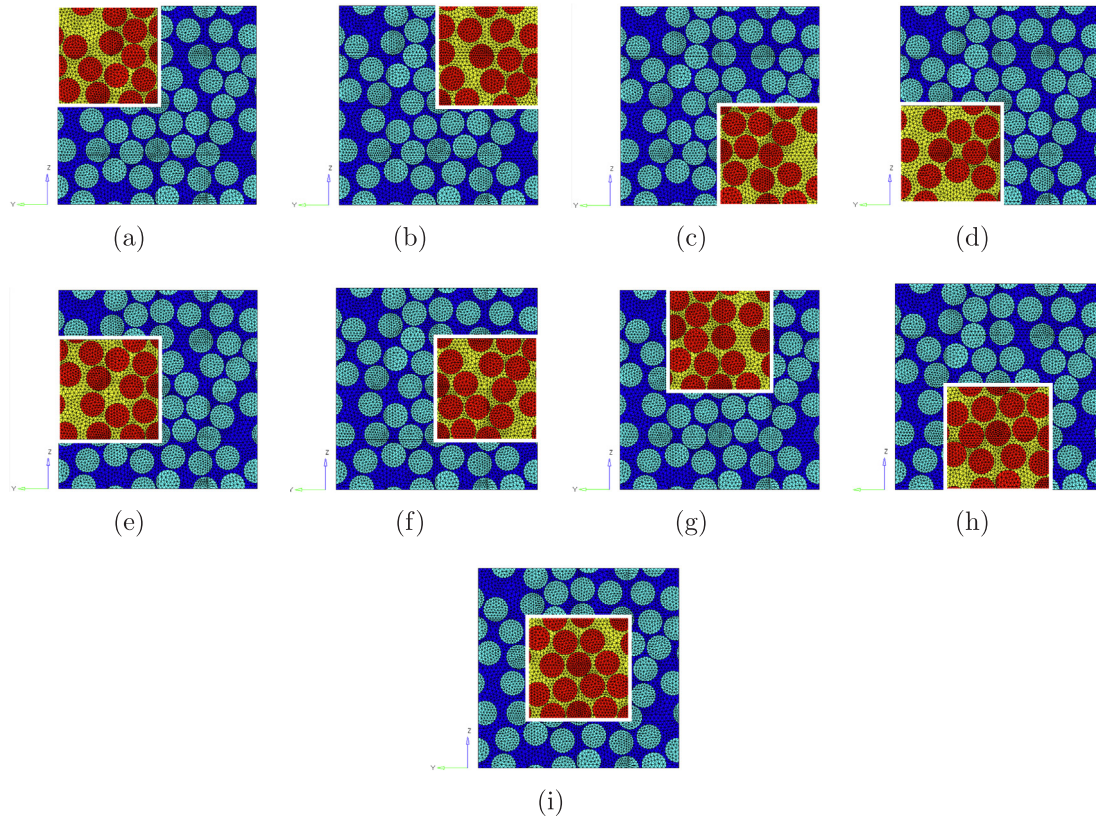


Fig. 28. RVEs with combination of four superframes for master RVE – model 1. (a) Window ABCD, (b) Window EFJK, (c) Window GLMN, (d) Window HIOP, (e) Window CDHI, (f) Window FGKL, (g) Window BCEF, (h) Window GHNO and (i) Window CFGH.

Table 26

Effective properties of Master RVE with the combination of four super frames.

Window	Volume fraction		Effective properties								
	V_f	V_m	E_1 (GPa)	E_2 (GPa)	E_3 (GPa)	G_{12} (GPa)	G_{13} (GPa)	G_{23} (GPa)	ν_{12}	ν_{13}	ν_{23}
Window ABCD	61.30	38.70	142.79	15.17	15.11	6.27	6.39	5.30	0.29	0.29	0.43
Window EFJK	59.52	40.48	138.79	14.86	15.79	5.77	6.31	5.03	0.30	0.29	0.40
Window HIOP	55.92	44.08	130.65	14.42	14.99	5.61	5.98	5.03	0.30	0.29	0.41
Window GLMN	62.00	38.00	144.36	15.01	15.83	6.11	6.72	5.30	0.29	0.29	0.41
Window CDHI	62.32	37.68	145.06	15.47	15.23	6.31	6.18	5.17	0.29	0.29	0.42
Window FGKL	64.20	35.80	149.33	15.71	15.98	6.40	6.51	5.16	0.29	0.29	0.40
Window CFGH	67.02	32.98	155.69	15.95	16.91	6.38	6.97	5.14	0.29	0.29	0.38
Window BCEF	64.96	35.04	151.04	15.57	17.25	5.89	7.18	4.99	0.30	0.29	0.36
Window GHNO	65.52	34.48	151.97	14.90	17.05	5.99	7.23	5.34	0.30	0.29	0.38
(μ)	62.48	37.52	145.52	15.24	16.02	6.09	6.61	5.17	0.29	0.29	0.40
(σ)	3.36	3.36	7.63	0.48	0.86	0.28	0.45	0.13	0.00	0.00	0.02
(ζ)	5.37	8.95	5.24	3.18	5.40	4.64	6.74	2.46	0.65	0.84	5.41

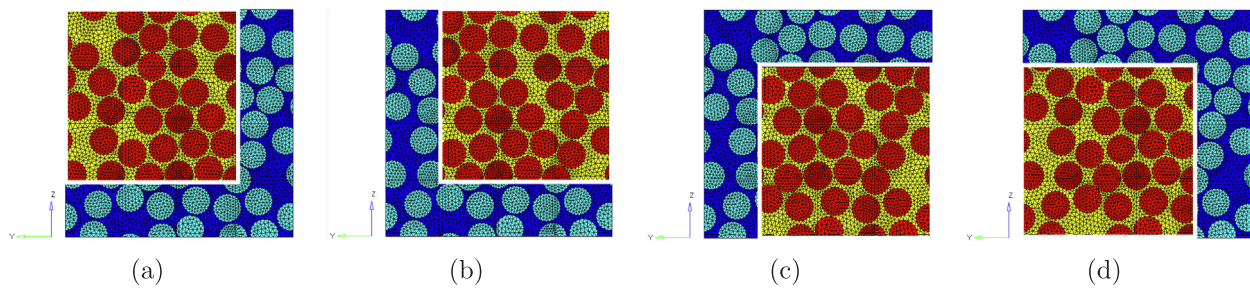


Fig. 29. RVEs with combination of eight superframes for master RVE – model 1. (a) Window ABCDEFGHI, (b) Window BCEFGHJKL, (c) Window CFGHKL MNO and (d) Window CDFGHINOP.

Table 27
Effective properties of Master RVE with the combination of eight super frames.

Window	Volume fraction		Effective properties								
	V_f	V_m	E_1 (GPa)	E_2 (GPa)	E_3 (GPa)	G_{12} (GPa)	G_{13} (GPa)	G_{23} (GPa)	ν_{12}	ν_{13}	ν_{23}
Window ABCDEFGHI	61.30	38.70	142.79	15.21	15.57	6.09	6.41	5.16	0.29	0.29	0.41
Window BCEFGHJKL	64.06	35.94	149.00	15.34	16.44	6.08	6.82	5.19	0.30	0.29	0.36
Window CDFGHINOP	61.62	38.38	143.52	15.09	15.74	6.05	6.47	5.17	0.29	0.29	0.42
Window CFGHKL MNO	63.06	36.94	146.77	15.31	16.32	6.09	6.73	5.14	0.29	0.30	0.41
(μ)	62.51	37.49	145.52	15.24	16.02	6.09	6.61	5.17	0.29	0.29	0.40
(σ)	1.28	1.28	2.89	0.11	0.43	0.02	0.20	0.02	0.00	0.00	0.03
(ζ)	2.05	3.42	1.99	0.73	2.67	0.30	2.97	0.38	0.30	1.65	6.37

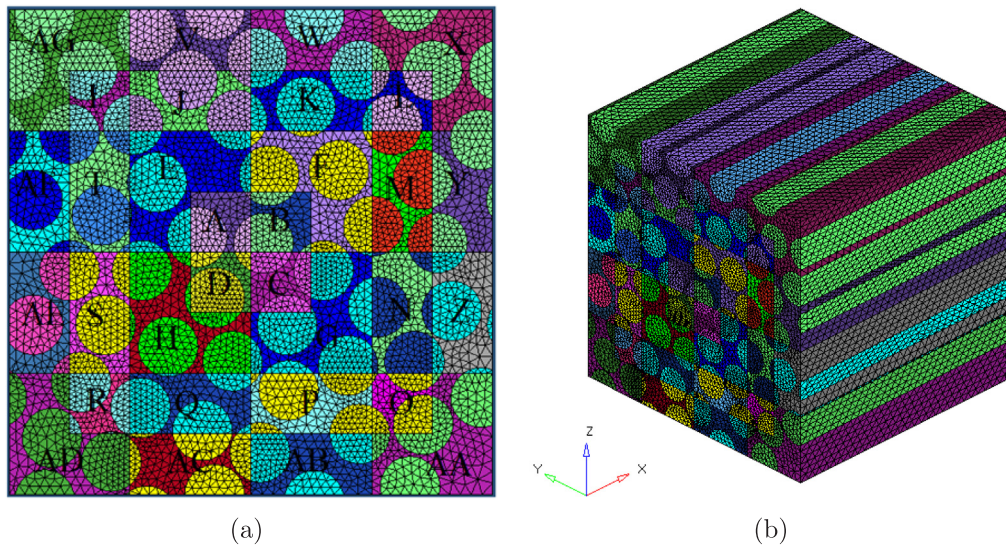


Fig. 30. Master RVE model 2. (a) Master RVE with the effect of local volume fraction (front view), (b) Master RVE with the effect of local volume fraction (isometric view).

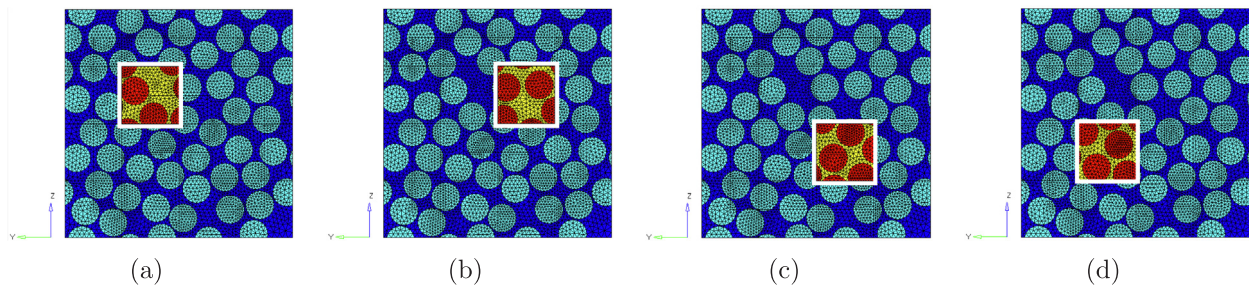


Fig. 31. RVEs with windows at the interior of the master RVE – model 2. (a) Window AE, (b) Window BF, (c) Window CG and (d) Window DH.

Table 28
Effective properties of different windows at the interior of the RVE.

Window	Volume fraction		Effective properties								
	V_f	V_m	E_1 (GPa)	E_2 (GPa)	E_3 (GPa)	G_{12} (GPa)	G_{13} (GPa)	G_{23} (GPa)	ν_{12}	ν_{13}	ν_{23}
Window AE	50.64	49.36	118.76	13.34	14.38	5.20	6.26	5.06	0.30	0.29	0.44
Window DH	68.11	31.89	158.14	15.88	15.21	6.67	6.34	5.36	0.29	0.29	0.43
Window BF	59.15	40.85	137.95	13.27	15.05	5.40	6.61	5.34	0.30	0.29	0.42
Window CG	64.59	35.41	150.20	15.58	14.76	6.64	6.07	5.40	0.29	0.29	0.44
(μ)	60.62	39.38	141.56	14.52	14.85	5.98	6.32	5.29	0.29	0.29	0.43
(σ)	7.61	7.61	17.15	1.41	0.37	0.79	0.22	0.16	0.01	0.00	0.01
(ζ)	12.55	19.32	12.14	9.69	2.47	13.15	3.55	2.97	1.79	1.00	2.94

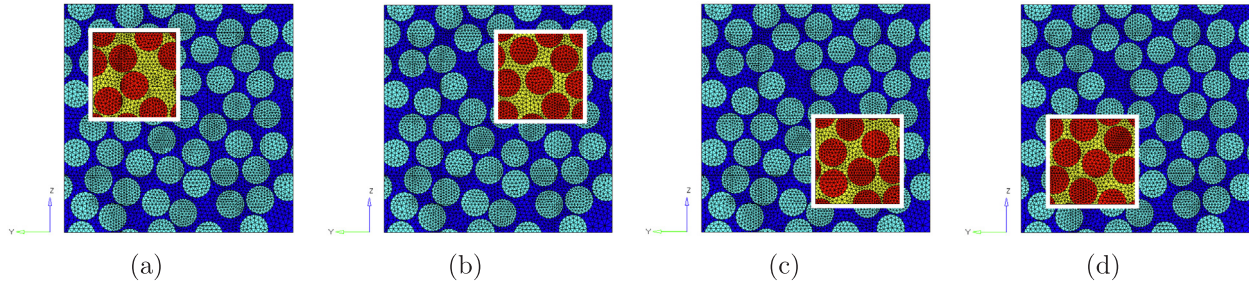


Fig. 32. RVEs with windows near the boundary of the master RVE – model 2. (a) Window AELJT, (b) Window BFKLM, (c) Window CGNOP and (d) Window DHQRS.

Table 29
Effective properties of different windows near the boundary of the RVE.

Window	Volume fraction		Effective properties								
	V_f	V_m	E_1 (GPa)	E_2 (GPa)	E_3 (GPa)	G_{12} (GPa)	G_{13} (GPa)	G_{23} (GPa)	ν_{12}	ν_{13}	ν_{23}
Window AELJT	57.77	42.23	134.84	14.07	15.05	5.62	6.48	5.21	0.30	0.29	0.42
Window DHQRS	66.36	33.64	154.19	15.75	16.01	6.43	6.82	5.27	0.29	0.29	0.40
Window CGNOP	63.19	36.81	147.05	15.82	15.34	6.56	6.26	5.25	0.29	0.29	0.42
Window BFKLM	64.33	35.67	149.61	14.49	15.47	6.02	6.69	5.50	0.29	0.29	0.42
(μ)	62.91	37.09	146.42	15.03	15.47	6.16	6.56	5.30	0.29	0.29	0.42
(σ)	3.67	3.67	8.27	0.88	0.40	0.43	0.25	0.13	0.00	0.00	0.01
(ζ)	5.83	9.89	5.56	5.88	2.58	6.92	3.76	2.47	0.90	0.53	2.16

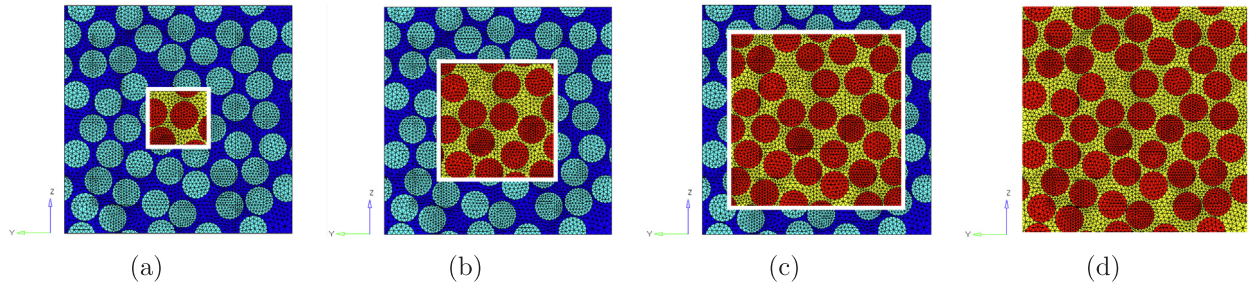


Fig. 33. RVEs with windows gradually increasing the window size of master RVE model 2. (a) Window ABCD, (b) Window ABCDEFGH, (c) Window ABST and (d) Window FULL RVE.

Table 30
Effective properties of the windows from interior to the whole RVE.

Window	Volume fraction		Effective properties								
	V_f	V_m	E_1 (GPa)	E_2 (GPa)	E_3 (GPa)	G_{12} (GPa)	G_{13} (GPa)	G_{23} (GPa)	ν_{12}	ν_{13}	ν_{23}
Window ABCD	58.80	41.20	137.17	14.33	15.17	5.88	6.37	5.24	0.29	0.29	0.41
Window ABCDEFGH	60.62	39.38	141.26	14.52	14.87	5.98	6.33	5.29	0.29	0.29	0.43
Window AB..ST	62.91	37.09	146.42	15.03	15.48	6.16	6.56	5.31	0.29	0.29	0.42
Window FULL RVE	59.66	40.34	139.10	14.58	14.89	6.02	6.28	5.33	0.29	0.29	0.42
(μ)	60.50	39.50	140.99	14.62	15.10	6.01	6.38	5.29	0.29	0.29	0.42
(σ)	1.77	1.77	3.99	0.30	0.28	0.12	0.13	0.04	0.00	0.00	0.01
(ζ)	4.58	6.77	8.36	9.19	7.03	9.99	7.27	7.15	0.52	0.65	1.98

- The out of plane properties show significant difference, mainly in ν_{23} . ν_{23} shows a variance of 30% with the experimental results for the RVE with fifty fibres. It could be the effect of free edges and effect of inter ply boundary layers that changes the observed experimental values. Again, this could be an outcome of the particular experiment used to obtain ν_{23} .
- As the RVE becomes more statistically homogeneous with the inclusion of more randomly distributed fibres, (along with cross

section variations), the properties approach the experimental values with improved transverse properties. However, the difference in computed and experimental values of transverse properties E_2 , ν_{23} , G_{23} does not go down and points to a need to relook at how these properties are obtained experimentally. Interestingly, experimental results mentioned in the literature [17] are mostly two dimensional, note that the micromechanical analysis in this study is three dimensional.

The other conclusions that can be drawn are listed as:

1. In particular, the percentage change of predicated G_{23} reduces from 22% (RVE with single fibre) to 10% (RVEs with 50 fibres). A similar trend is seen for other shear moduli, suggesting that randomness gives a more realistic representation of micro-structure.
2. The percentage change for transverse Poisson's ratio ν_{23} reduces from 35% (RVE with single fibre) to 30% (RVEs with 50 fibres).
3. For the RVE with random fibre distribution, shielding effect of neighbouring fibres is accounted for, which is missing in the single fibre RVE.
4. For the master RVE it is seen that the effect of volume fraction plays a vital role in predicted effective properties. The fibre rich and matrix rich regions have a significant effect of the predicted effective properties and the axial modulus, E_1 significantly changes with the change in local volume fraction.

Appendix A. Supplementary data

Supplementary data associated with this article can be found, in the online version, at <https://doi.org/10.1016/j.compstruct.2019.111141>.

References

- [1] Daniel IM, Ishai O, Daniel IM, Daniel I. *Engineering Mechanics of Composite Materials* vol. 3. New York: Oxford University Press; 1994.
- [2] Jones RM. *Mechanics of Composite Materials* vol. 193. DC: Scripta Book Company Washington; 1975.
- [3] Hashin Z, Herakovich CT, Weitsman Y. *Mechanics of composite materials: recent advances*. *J Appl Mech* 1984;51:224.
- [4] Aboudi J, Arnold SM, Bednarczyk BA. *Micromechanics of composite materials: a generalized multiscale analysis approach*. Butterworth-Heinemann; 2012.
- [5] Trias D, Costa J, Mayugo J, Hurtado J. Random models versus periodic models for fibre reinforced composites. *Comput Mater Sci* 2006;38(2):316–24.
- [6] Gitman I, Askes H, Sluys L. Representative volume: existence and size determination. *Eng Fract Mech* 2007;74(16):2518–34.
- [7] Kani T, Forest S, Galliet I, Mounoury V, Jeulin D. Determination of the size of the representative volume element for random composites: statistical and numerical approach. *Int J Solids Struct* 2003;40(13):3647–79.
- [8] Buryachenko V, Pagano N, Kim R, Spowart J. Quantitative description and numerical simulation of random microstructures of composites and their effective elastic moduli. *Int J Solids Struct* 2003;40(1):47–72.
- [9] Pyrz R. Quantitative description of the microstructure of composites. part i: Morphology of unidirectional composite systems. *Compos Sci Technol* 1994;50(2):197–208.
- [10] H.T.D. Kleiber M. *The stochastic finite element method*, John Wiley and Sons.
- [11] Takano N, Uetsuji Y, Kashiwagi Y, Zako M. Hierarchical modelling of textile composite materials and structures by the homogenization method. *Modell Simul Mater Sci Eng* 1999;7(2):207.
- [12] Pyrz R. Correlation of microstructure variability and local stress field in two-phase materials. *Mater Sci Eng: A* 1994;177(1–2):253–9.
- [13] Sriramula S, Chryssanthopoulos MK. Quantification of uncertainty modelling in stochastic analysis of FRP composites. *Compos Part A: Appl Sci Manuf* 2009;40(11):1673–84.
- [14] Yushanov SP, Bogdanovich AE. Stochastic theory of composite materials with random waviness of the reinforcements. *Int J Solids Struct* 1998;35(22):2901–30.
- [15] Tyrus J, Gosz M, DeSantiago E. A local finite element implementation for imposing periodic boundary conditions on composite micromechanical models. *Int J Solids Struct* 2007;44(9):2972–89.
- [16] Soden P, Hinton M, Kaddour A. Lamina properties, lay-up configurations and loading conditions for a range of fibre-reinforced composite laminates. *Compos Sci Technol* 1998;58(7):1011–22.
- [17] Hinton MJ, Kaddour AS, Soden PD. *Failure criteria in fibre reinforced polymer composites: the world-wide failure exercise*. Elsevier; 2004.
- [18] Aboudi J. *Mechanics of Composite Materials: a unified micromechanical approach* vol. 29. Elsevier; 2013.
- [19] Melro A, Camanho P, Pinho S. Generation of random distribution of fibres in long-fibre reinforced composites. *Compos Sci Technol* 2008;68(9):2092–102.
- [20] Yang L, Yan Y, Ran Z, Liu Y. A new method for generating random fibre distributions for fibre reinforced composites. *Compos Sci Technol* 2013;76:14–20.
- [21] Hill R. Theory of mechanical properties of fibre-strengthened materials: I. Elastic behaviour. *J Mech Phys Solids* 1964;12(4):199–212.
- [22] Drugan W, Willis J. A micromechanics-based nonlocal constitutive equation and estimates of representative volume element size for elastic composites. *J Mech Phys Solids* 1996;44(4):497–524.
- [23] Ostoja-Starzewski M. Random field models of heterogeneous materials. *Int J Solids Struct* 1998;35(19):2429–55.
- [24] Bakhvalov NS, Panasenko G. *Homogenisation: averaging processes in periodic media: mathematical problems in the mechanics of composite materials* vol. 36. Springer Science & Business Media; 2012.
- [25] Kalamkarov AL. *Composite and reinforced elements of constructions*. Baffins Lane, Chichester, West Sussex PO 19 1 UD, UK: John Wiley & Sons Ltd; 1992. 286.
- [26] Oleinik OA, Shamaev A, Yosifian G. *Mathematical problems in elasticity and homogenization* vol. 26. Elsevier; 1992.
- [27] Suquet P. *Elements of homogenization for inelastic solid mechanics*. Homogenization Tech Compos Media 1987;272:193–278.
- [28] Terada K, Hori M, Kyoya T, Kikuchi N. Simulation of the multi-scale convergence in computational homogenization approaches. *Int J Solids Struct* 2000;37(16):2285–311.
- [29] Murari V, Upadhyay C. Micromechanics based diffuse damage model for unidirectional composites. *Compos Struct* 2013;96:419–32.
- [30] Babuška I. *Homogenization approach in engineering. Computing methods in applied sciences and engineering*. Springer; 1976. p. 137–53.
- [31] Kalamkarov AL, Andrianov IV, Danishevskii VV, et al. Asymptotic homogenization of composite materials and structures. *Appl Mech Rev* 2009;62(3):030802.
- [32] Venkat SM. A comparative study of the micromechanics models in predicting effective mechanical properties of fibrous composites. Indian Institute of Technology Kanpur 2013. (M.Tech dissertation).